HHS Public Access

Author manuscript

Cell Rep. Author manuscript; available in PMC 2020 December 11.

Published in final edited form as:

Cell Rep. 2020 November 10; 33(6): 108370. doi:10.1016/j.celrep.2020.108370.

Ppargc1a Controls Ciliated Cell Development by Regulating Prostaglandin Biosynthesis

Joseph M. Chambers[1,*], **Amanda Addiego**[1], **Ana L. Flores-Mireles**[2], **Rebecca A. Wingert**[1,3,*]

[1]Department of Biological Sciences, Center for Stem Cells and Regenerative Medicine, Center for Zebrafish Research, Boler-Parseghian Center for Rare and Neglected Diseases, University of Notre Dame, Notre Dame, IN 46556, USA

[2]Department of Biological Sciences, Eck Institute for Global Health, University of Notre Dame, Notre Dame, IN 46556, USA

[3]Lead Contact

SUMMARY

Cilia are microtubule-based organelles that function in a multitude of physiological contexts to perform chemosensing, mechanosensing, and fluid propulsion. The process of ciliogenesis is highly regulated, and disruptions result in disease states termed ciliopathies. Here, we report that *peroxisome proliferator-activated receptor gamma, coactivator 1 alpha* (*ppargc1a*) is essential for ciliogenesis in nodal, mono-, and multiciliated cells (MCCs) and for discernment of renal tubule ciliated cell fate during embryogenesis. *ppargc1a* performs these functions by affecting prostaglandin signaling, whereby cilia formation and renal MCC fate are restored with prostaglandin E_2 (PGE_2) treatment in *ppargc1a*-deficient animals. Genetic disruption of *ppargc1a* specifically reduces expression of the prostanoid biosynthesis gene *prostaglandin-endoperoxide synthase 1* (*ptgs1*), and suboptimal knockdown of both genes shows this synergistic effect. Furthermore, *ptgs1* overexpression rescues ciliogenesis and renal MCCs in *ppargc1a*-deficient embryos. These findings position Ppargc1a as a key genetic regulator of prostaglandin signaling during ciliated cell ontogeny.

In Brief

Prostaglandin signaling has key roles in ciliated cell fate decisions during nephron development as well as the process of ciliogenesis. Chambers et al. show that activity of Ppargc1a regulates ciliogenesis in zebrafish embryos by controlling production of the prostaglandin PGE_2 via the prostaglandin pathway component Ptgs1.

*Correspondence: jmchambers@manchester.edu (J.M.C.), rwingert@nd.edu (R.A.W.).

AUTHOR CONTRIBUTIONS

J.M.C. and R.A.W. designed the experiments. J.M.C., A.A., and A.L.F.-M. performed experiments. J.M.C., A.A., A.L.F.-M., and R.A.W. analyzed results and wrote and revised the paper.

DECLARATION OF INTERESTS

The authors declare no competing interests.

SUPPLEMENTAL INFORMATION

Supplemental Information can be found online at https://doi.org/10.1016/j.celrep.2020.108370.

Graphical Abstract

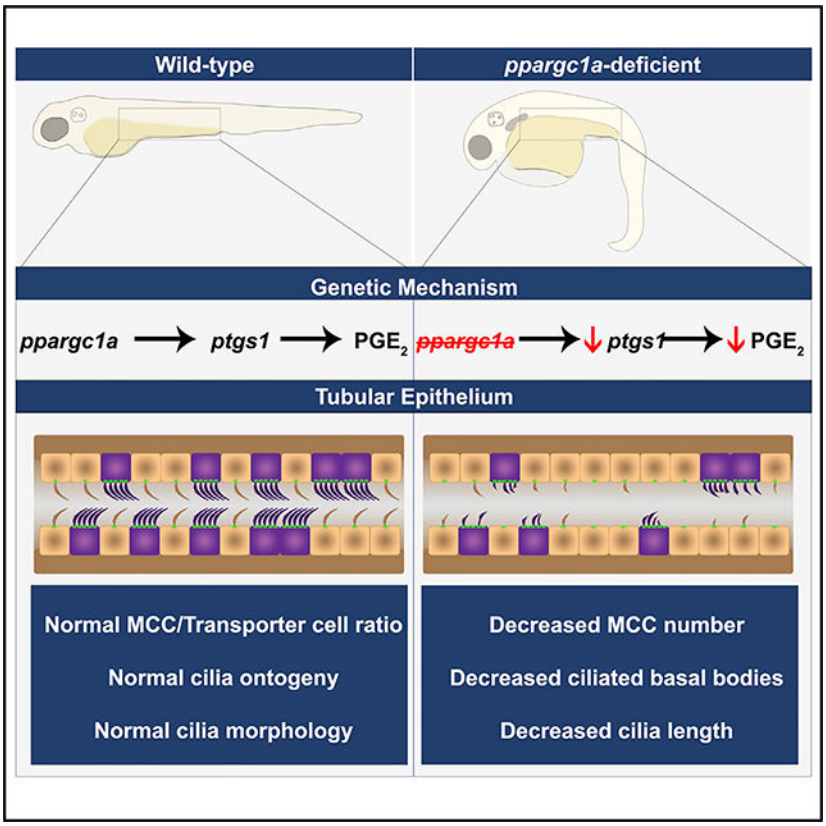

INTRODUCTION

Cilia are hair-like structures that project from the cell surface, where they perform extremely important tasks including chemosensing, mechanosensing, and fluid propulsion. Although most vertebrate cells possess a single immotile cilium, others are specialized to be motile multiciliated cells (MCCs) (Marra et al., 2016). Nodal cilia are a unique third class of ciliated cells that are transient and include a single motile cilium necessary for establishing left-right symmetry across vertebrates (Essner et al., 2002). Cilia structures consist of an axoneme, basal body, transition zone, ciliary membrane, and ciliary tip (Fliegauf et al., 2007). Disruptions to these ciliary structures are linked to heterogeneous human diseases termed ciliopathies, which are characterized by multisystem defects in organs such as the brain, heart, lungs, and kidneys (Mitchison and Valente, 2017; Reiter and Leroux, 2017). Despite recent advances in identifying steps of ciliogenesis, continued elucidation of the genetic mechanisms that regulate cilia structure and function, as well as the discernment of monociliated versus MCC fate, remain areas of central importance.

Several studies have highlighted key roles for prostaglandin signaling in ciliated cell ontogeny. During ciliogenesis, binding of bioactive prostanoid prostaglandin E_2 (PGE_2) to its receptor EP4 triggers a cyclic AMP-mediated signaling cascade, which promotes anterograde intraflagellar transport (IFT) of protein cargoes that extend cilia (Jin et al.,

2014). Disruption of prostaglandin synthesis also leads to probasal body accumulation during multiciliogenesis, suggesting a role in regulating their trafficking or docking to the cell surface (Marra et al., 2019a). Additionally, prostaglandin signaling is necessary for renal progenitors in the zebrafish embryonic kidney, or pronephros, to adopt an MCC fate during nephron development, where a monociliated cell fate is chosen preferentially in the absence of normal prostaglandin synthesis (Marra et al., 2019a).

Interestingly, levels of PGE_2 in the adult mammalian kidney are directly related to levels of *peroxisome proliferator-activated receptor (PPAR) gamma, coactivator 1 alpha* (*PGC-1α*; also known as *Ppargc1a*), which provide renoprotective effects following injury (Tran et al., 2016). PGC-1α is best known as a coactivator for the PPAR pathway, though it is now appreciated to serve a number of diverse tissue-specific functions (Puigserver and Spiegelman, 2003; Chambers and Wingert, 2020). Among these, *ppargc1a* was recently discovered to mediate cell fate in the developing zebrafish embryo kidney (or pronephros) by controlling regionalized expression of several transcription factors to establish segment domains within nascent nephrons (Chambers et al., 2018). However, despite the connection between PGC-1α and PGE_2 in mature nephrons, there has been no previous evidence suggesting a relationship between these effectors during kidney or ciliated cell development.

Here, we report that *ppargc1a* is necessary for both proper ciliogenesis and MCC specification. *ppargc1a* zebrafish mutants and morphants exhibited cilium loss and/or shortened cilia in several tissues, including the ear, Kupffer's vesicle (KV), and pronephros. *ppargc1a*-deficient embryos also displayed reduced numbers of renal MCCs, while monociliated cell numbers increased, thereby recapitulating the effects of attenuated prostaglandin signaling. Thus, we tested the hypothesis that these pathways were connected and found that PGE_2 metabolites were decreased in *ppargc1a*-deficient zebrafish and that MCC fate choice and cilia length were restored in *ppargc1a*-deficient embryos treated with $dmPGE_2$. Genetic interaction studies revealed a synergistic effect between *ppargc1a* and the prostaglandin biosynthesis enzyme encoded by *prostaglandin-endo-peroxide synthase 1* (*ptgs1*; also known as *cyclooxygenase*; [*cox1*]), where combined suboptimal knockdowns resulted in ciliated cell defects. Consistent with these findings, *ppargc1a*-deficient embryos exhibited decreased *ptgs1* transcript levels, where provision of *ptgs1* mRNA was sufficient to rescue MCC number and cilia length. These results advance our fundamental understanding of ciliated cell patterning and differentiation by illuminating pivotal roles for *ppargc1a* in regulating prostaglandin production.

RESULTS

ppargc1a-Deficient Zebrafish Exhibit Ciliopathic Phenotypes

Hallmarks of underlying ciliary defects in the zebrafish embryo commonly present as pleiotropic phenotypes, including pronephric cysts, curved body axes, and edema (Drummond et al., 1998; Sun et al., 2004; Kramer-Zucker et al., 2005; Sullivan-Brown et al., 2008). Subsequent to detailing the role *ppargc1a* plays in nephron segmentation (Chambers et al., 2018), we unexpectedly detected a suite of morphological phenotypes suggestive of ciliary dysfunction in $ppargc1a^{sa13186/sa13186}$ mutants. $ppargc1a^{sa13186}$ zebrafish (ZIRC) have a T-to-A mutation resulting in a premature stop codon in exon 7 (Chambers et al.,

2018). At about 48 h post-fertilization (hpf), *ppargc1a*$^{sa13186/sa13186}$ zebrafish developed curly tails, pronephric cysts, and pericardial edema compared with wild-type (WT) siblings (Figures 1A and 1B). These surprising phenotypes presented in a manner following the expected Mendelian ratio for a recessive allele bred through heterozygous incrosses (Figure 1A). Additionally, *ppargc1a*$^{sa13186/sa13186}$ mutant embryos had atypical otic vesicle formation at 3 days post-fertilization (dpf), including the number of otoliths formed (Figure 1C) and diminished cilia formation on the cristae structures at 4 dpf (Figure 1D) (Wu et al., 2011; Yu et al., 2011; Stooke-Vaughan et al., 2012).

To further investigate the function of the pronephros, we microinjected 40 kDa dextran-FITC (fluorescein isothiocyanate) into 48 hpf WT and *ppargc1a*$^{sa13186/sa13186}$ mutant embryos, then imaged the animals at the 72 hpf stage. Whereas WT embryos exhibited strong fluorescence signal in the proximal convoluted tubule (PCT), indicating normal fluid flow, *ppargc1a*$^{sa13186/sa13186}$ mutants failed to take up the fluorescent conjugate (Figure 1E). Lack of fluid flow from ciliary defects disrupts collective cell migration and PCT morphogenesis in the pronephros (Vasilyev et al., 2009). Thus, to determine if the PCT was forming correctly, we performed whole-mount *in situ* hybridization (WISH) for *slc20a1a* and found a lack of coiling morphogenesis in *ppargc1a*$^{sa13186/sa13186}$ compared with WT siblings (Figure 1F). These data suggest that cilia in the pronephros are not functioning properly.

Several studies of the KV have illustrated that the establishment of left-right symmetry is affected by loss of cilia function (Essner et al., 2005; Wang et al., 2011, 2012; Compagnon et al., 2014; Dasgupta and Amack, 2016). To assess left-right patterning in *ppargc1a*-deficient embryos, we examined its first overt morphological feature in vertebrates, cardiac looping. Using a previously validated *ppargc1a* morpholino oligonucleotide (MO) (Chambers et al., 2018), we performed WISH for the heart marker *myl7* at 55 hpf and found that a randomization of heart looping occurred in *ppargc1a* morphants compared with WT controls (Figure 1G) (Bisgrove et al., 2005; Tian et al., 2009; Huang et al., 2011; Manning et al., 2013). To determine if the randomization of cardiac looping correlated with changes in KV cilia formation, we performed whole-mount immunofluorescence (IF) at the 10 somite stage (ss). Because KV phenotypes largely depend on age, we ensured that each sample was 10 ss before fixation. Subsequent analysis revealed that both the number and length of cilia in the KV were decreased in *ppargc1a* morphants compared with WTs (Figures 1H–1J).

Given these observations, we examined if the expression of *ppargc1a* and/or Ppargc1a corresponded with ciliated cell populations in the embryo. Previous reports have shown that *ppargc1a* transcripts are expressed in the renal progenitor field (Bertrand et al., 2007; Chambers et al., 2018). WISH studies in 24 hpf WT embryos confirmed that *ppargc1a* transcripts were spatially localized to the pronephros (Figure 1K) as well as another ciliated area, the nasal placodes (Figure 1K, inset). Interestingly, IF studies revealed that Ppargc1a protein is localized to the apical surface of the distal pronephros tubule cells (Figure 1K; Figure S1A). Taken together, these data suggest that *ppargc1a* is necessary for cilia formation, cilia function, or both, as it is expressed in ciliated areas, and zebrafish deficient in *ppargc1a* display multiple hallmarks of ciliopathies.

ppargc1a-Deficient Nephrons Have a Depleted MCC Lineage and Atypical Cilia Formation

On the basis of the renal phenotypes in *ppargc1a* mutants, we hypothesized that ciliated cell fate choice and/or ciliogenesis were compromised. The zebrafish pronephros has two types of ciliated cells that occupy the tubule: MCCs and monociliated transporter cells, where the latter includes several unique differentiated types that are organized into a series of discrete functional segments (Figure 2A) (Wingert et al., 2007; Liu et al., 2007; Ma and Jiang, 2007). Within the proximal tubule segments, MCCs are distributed in a “salt and pepper” fashion such that they are interspersed with the monociliated transporter populace. In contrast, the last distal tubule segment and pronephric duct regions are composed solely of monociliated transporter cells (Figure 2A) (Marra and Wingert, 2016). Both cell types possess motile cilia that function in fluid propulsion (Kramer-Zucker et al., 2005). Interestingly, *ppargc1a*-deficient animals have an increased proximal straight tubule (PST) segment, marked specifically by transcripts encoding *trpm7*, suggesting an increased number of monociliated transporter cells (Chambers et al., 2018). Furthermore, there is precedence that elevated monociliated cell number can occur at the expense of MCC fate choice (Marra et al., 2019a, 2019b).

Therefore, we first sought to determine if MCCs were developing properly in *ppargc1a*-deficient embryos. *ppargc1a* mutant zebrafish were assessed with WISH for the MCC marker *odf3b*, which showed that they had significantly fewer MCCs per nephron compared with WT control embryos (Figures 2B and 2C). Using fluorescent *in situ* hybridization (FISH) to enable precise quantification of both MCCs and monociliated cells, we found that *ppargc1a*-deficient embryos had a decreased number of *odf3b*$^{+}$ cells that was proportional to the increased number of *trpm7*$^{+}$ cells (Figures 2D–2F). Notably, the number of nuclei marked by DAPI in WT and *ppargc1a*-deficient embryos was not significantly different within this segment domain, suggesting that altered cell number and/or morphology does not account for the changes in MCC/transporter cell ratio (Figure S1B). Given the reduction in maturing MCCs, we used WISH to examine expression of the MCC progenitor marker *jag2b* (Marra et al., 2019a). *ppargc1a*-deficient embryos had significantly reduced numbers of *jag2b*$^{+}$ cells compared with WT controls (Figures S1C and S1D). These findings support the conclusion that fate choice between MCC and monociliated transport cell identity in the developing PST is altered as a consequence of *ppargc1a* deficiency.

Next we explored ciliary development in the pronephros using whole-mount IF to detect acetylated α-tubulin (cilia), γ-tubulin (basal bodies), and DAPI in WT and *ppargc1a*-deficient embryos at the 28 hpf stage. In the proximal pronephros, cilia length was significantly shorter in both *ppargc1a*$^{sa13186/sa13186}$ and *ppargc1a* morphant embryos compared with WT (Figures 2G and 2H). Additionally, we noted that *ppargc1a*-deficient embryos possessed fewer ciliated basal bodies (Figure 2I), suggesting a defect in initiating cilium formation. Consistent with reduced cilium formation and shorter cilium length, the fluorescent intensity of the acetylated α-tubulin signal was reduced in *ppargc1a*-deficient embryos compared with WT controls (Figure 2M). As the proximal pronephros is composed of MCCs and transporter cells, these data suggest ciliogenesis defects in both populations.

To investigate this further, we examined the distal tubule, as it consists of a homogeneous population of monociliated cells. Similar to the proximal tubule, cilia length in the distal

tubule domain was significantly decreased in *ppargc1a*-deficient embryos compared with WT controls (Figures 2J and 2K). Likewise, distal tubule cells in *ppargc1a*-deficient embryos possessed fewer ciliated basal bodies (Figure 2L). Furthermore, the fluorescent intensity of the acetylated α-tubulin signal was lower in *ppargc1a*-deficient embryos compared with WT controls, consistent with decreased cilia formation (Figure 2N). Taken together, these data documenting shortened or absent cilia in tubule cells of the proximal and distal pronephros indicate that cilia formation is significantly disrupted in two independent *ppargc1a*-deficient zebrafish models and support the conclusion that *ppargc1a* is requisite for proper ciliogenesis.

To assess if the MCC abrogation and defunct ciliogenesis phenotypes are related outcomes unique to *ppargc1a* deficiency, we examined MCC formation in *ift88*-deficient embryos. Loss of the IFT factor *ift88* in zebrafish, which is an ortholog of the mouse *Polaris* gene, causes cystic kidney, reduced cilia length, abrogated fluid flow in the pronephros, and randomized heart looping (Kramer-Zucker et al., 2005; Vasilyev et al., 2009; Manning et al., 2013; Gerlach and Wingert, 2014), mimicking cystic kidney disease and laterality randomization in mice with hypomorphic mutations in *Polaris* (Moyer et al., 1994; Yoder et al., 1995). Interestingly, MCC number was not significantly different between WT control embryos and *ift88* morphants (Figures S2A and S2B). This finding suggests that ciliogenesis and MCC fate choice are not intrinsically linked developmental pathways. Injection of a standard control MO also resulted in no significant changes to the number of MCCs, proximal and distal cilia length, or proximal and distal ciliated basal bodies (Figures S2C–S2J). Taken together, these data led us to conclude that *ppargc1a* deficiency specifically leads to two independent developmental defects in nephrons, namely, a depleted MCC population (that is replaced by an expanded monociliated transport cell populace) and atypical cilia formation.

Ciliogenesis and Renal MCC Fate in *ppargc1a*-Deficient Zebrafish Can Be Rescued by PGE_2

Recent studies have established that prostaglandin signaling is needed for proper cilium elongation, basal body trafficking, and MCC versus transporter cell fate choice during pronephros development (Jin et al., 2014; Marra et al., 2019a). Strikingly, *ppargc1a*-deficient embryos possess both the ciliogenesis and renal cell fate defects as embryos lacking prostaglandin signaling. A link between *ppargc1a* and the prostanoid PGE_2 was previously reported in the injured adult mammalian kidney, where decreased *ppargc1a* resulted in decreased PGE_2 levels and increased *ppargc1a* correlated with increased PGE_2 levels (Tran et al., 2016). Additionally, ciliary and renal abnormalities from defective prostaglandin synthesis or export are rescued by provision of PGE_2 or its analog 16,16-dimethyl-PGE_2 ($dmPGE_2$), the latter of which has a longer half-life (Jin et al., 2014; Poureetezadi et al., 2016; Marra et al., 2019a). Therefore, we hypothesized that *ppargc1a*-deficient animals lack sufficient PGE_2 and that supplementing with a form of PGE_2 during development might restore ciliogenesis and MCC fate choice.

First, to determine if *ppargc1a*-deficient zebrafish had decreased PGE_2, we performed an ELISA for PGE_2 metabolites (Esain et al., 2015). ELISA results indicated a significant

decrease in PGE_2 metabolites in 28 hpf *ppargc1a*-deficient zebrafish (Figure 3A). As prostaglandin signaling is necessary for MCC cell fate and maturation (Marra et al., 2019a), and *ppargc1a*-deficient embryos similarly have decreased MCC progenitors (*jag2b*$^+$ cells) and maturing MCCs (*odf3b*$^+$ cells) (Figures 2B and 2C; Figures S1C and S1D), we examined the effect of $dmPGE_2$ on MCC development in *ppargc1a*-deficient zebrafish. To do this, we completed WISH for *odf3b* in 24 hpf stage WT controls, *ppargc1a* morphants, and *ppargc1a* morphants supplemented with 100 μM $dmPGE_2$ (Figure 3B). The *ppargc1a* morphant model was selected for these studies because we had not observed any discernible phenotype differences between mutant and morphant embryos (Figures 1 and 2). Importantly, the use of morphants is highly tractable, as it enabled us to reduce the number of animals needed for experiments and increased the efficiency of the studies because this approach does not necessitate genotyping. $dmPGE_2$ rescued MCC number in *ppargc1a*-deficient embryos to WT levels (Figures 3B and 3C). Furthermore, changing the time of addition for $dmPGE_2$ supplementation to 8, 10, or 12 hpf led to comparable rescue of MCC number in *ppargc1a*-deficient embryos (Figure S3A). We observed no gain-of-function phenotype in the number of MCCs (Figure S3B), suggesting that there is a threshold above which normal MCCs develop.

Next, to test if $dmPGE_2$ treatment could rescue the ciliogenesis phenotypes observed in *ppargc1a* deficiency, we treated *ppargc1a*-deficient embryos with 100 μM $dmPGE_2$ beginning at 6 hpf, and pronephros ciliogenesis was assessed at 28 hpf using whole-mount IF. In the proximal tubule, $dmPGE_2$ rescued the appearance of cilia in *ppargc1a*-deficient embryos compared with vehicle-treated controls (Figure 3D). Quantification of ciliary length showed a significant restoration in the $dmPGE_2$-treated *ppargc1a* morphants (Figure 3E), which was consistent with measurements of cilia fluorescent intensity (Figure 3J). Additionally, the number of ciliated basal bodies in $dmPGE_2$-treated *ppargc1a* morphants was restored to a WT level (Figure 3F). Evaluation of these features in WT embryos treated with $dmPGE_2$ did not reveal a gain-of-function effect (Figures S3C and S3D). These findings suggested that cilia formation in monociliated cells and MCCs in *ppargc1a*-deficient embryos is rescued by provision of a bioactive PGE_2 prostanoid. Similar analyses were performed in the distal pronephros to explicitly examine if ciliogenesis in monociliated cells of this region was similarly restored (Figure 3G). Again, we observed an overt rescue of ciliogenesis in $dmPGE_2$-treated *ppargc1a* morphants compared with vehicle controls (Figure 3G), which was significant when ciliary length and ciliated basal bodies were quantified (Figures 3H and 3I), and consistent with measurements of cilia fluorescent intensity (Figure 3K). Together, these findings led us to conclude that ciliogenesis throughout the pronephros was restored in *ppargc1a*-deficient animals by addition of $dmPGE_2$.

Furthermore, we investigated if $dmPGE_2$ supplementation was sufficient to rescue the curved body axis phenotype observed at the 48 hpf stage. We obtained three independent clutches from matings of *ppargc1a*$^{+/sa13186}$ heterozygous adults, then split each clutch at 6 hpf to treat half of the embryos with media containing DMSO vehicle, while the other half were immersed in media with $dmPGE_2$; subsequently, the media was refreshed at 24 and 33 hpf to offset degradation of the prostanoid. At the 48 hpf stage, DMSO-treated cohorts displayed the expected Mendelian ratio (25%) of mutant phenotype with 24.33% curly, and

the corresponding $dmPGE_2$-treated cohorts displayed an incidence of mutant phenotype with 13% curly (Figures 3L and 3M). Representative genotype analysis of random embryos from each cohort confirmed that some *ppargc1a*$^{sa13186/sa13186}$ mutants displayed WT morphology following $dmPGE_2$ administration (Figure 3L). We concluded that the regimen of $dmPGE_2$ supplementation rescued ciliogenesis in some cases, and we speculate that rescue of all mutants was not obtained even with fresh additions during the experiment, likely because of fluctuations in the quantity of active $dmPGE_2$ over this protracted developmental interval. In sum, these data show that provision of $dmPGE_2$ is sufficient to rescue ciliogenesis and renal MCC fate choice in *ppargc1a*-deficient zebrafish.

ppargc1a Regulates the Prostaglandin Pathway Component *ptgs1*

Prostaglandin synthesis occurs when a cyclooxygenase enzyme (Cox1 or Cox2) converts arachidonic acid to an intermediate that is subsequently converted to an active prostanoid such as PGE_2. Compromised prostanoid biosynthesis due to the loss of *ptgs1*, which encodes Cox1 in zebrafish, abrogates ciliogenesis and skews renal MCC fate choice (Marra et al., 2019a). Therefore, we designed genetic interaction studies to explore the relationship between *ppargc1a* and *ptgs1*. Suboptimal doses of MOs are commonly used to test for a synergistic effect that would suggest multiple genes act in a shared pathway (DiBella et al., 2009; Wagle et al., 2011; Choi et al., 2015; Kallakuri et al., 2015). We conducted suboptimal MO (SMO) microinjections with *ppargc1a* and *ptgs1* on the basis of previously established dosages (North et al., 2007; Jin et al., 2014; Esain et al., 2015; Poureetezadi et al., 2016; Chambers et al., 2018; Marra et al., 2019a). Furthermore, we performed IF to evaluate Ppargc1a expression following *ppargc1a* SMO, which revealed diminished signal in the distal pronephros (Figure S1A), which was statistically significant when quantified on the basis of fluorescent intensity (Figure S4A). Assessment of ciliogenesis using IF in the proximal pronephros (Figures 4A–4C) and distal pronephros (Figures 4D–4F) revealed no statistical difference in cilia length or ciliated basal bodies in WT, *ppargc1a* SMO, or *ptgs1* SMO, while there was a statistically significant decrease in *ppargc1a* + *ptgs1* SMO. Additionally, the mean fluorescent intensity was lower for the combination knockdown compared with WT or single knockdowns (Figures S4B and S4C). Next, we tested the effect of incubating *ppargc1a* + *ptgs1* SMO knockdowns with $dmPGE_2$. Addition of $dmPGE_2$ rescued cilia length, the percentage of ciliated basal bodies, and cilia fluorescent intensity in the proximal (Figures 4A–4C; Figure S4B) and distal pronephros (Figures 4D–4F; Figure S4C).

Because previous research identified an essential role for *ptgs1* in MCC development (Marra et al., 2019a), we investigated if the *ppargc1a*/*ptgs1* relationship was relevant to MCC fate choice. WISH was used to detect expression of the MCC marker *odf3b*, in WT, *ppargc1a* SMO, *ptgs1* SMO, and the *ppargc1a* + *ptgs1* SMO (Figure 4G). Significantly decreased MCC numbers were observed in *ppargc1a* SMO and *ptgs1* SMO compared with WT controls (Figures 4G and 4H). MCC number in *ppargc1a* + *ptgs1* SMO embryos was significantly less than the quantity seen in either single SMO injected group, excluding an additive consequence (Figures 4G and 4H). Furthermore, MCC number was rescued with the addition of $dmPGE_2$ in *ppargc1a* + *ptgs1* SMO embryos (Figures 4G and 4H). These

data provide evidence of a synergistic effect on renal MCC fate choice in the context of *ppargc1a* and *ptgs1* suboptimal knockdown.

As loss of *ppargc1a* or *ptgs1* results in morphological defects, including a curved body, we also performed live imaging studies with our suboptimal knockdown model. The combined loss of *ppargc1a* and *ptgs1* dramatically increased the incidence of embryos with affected phenotypes (curved body axis) compared with single SMO knockdowns (Figure 4I; Figure S4D). Additionally, the number of affected *ppargc1a* + *ptgs1* SMO embryos was nearly eliminated following $dmPGE_2$ treatment (Figure 4I; Figure S4D). Overall, this evidence strongly indicated a link between *ppargc1a* and *ptgs1* in ciliogenesis and MCC development in the pronephros.

To further interrogate the relationship between *ppargc1a* and *ptgs1*, we examined the promoter region 1.5 kb upstream of the *ptgs1* start site. Our analysis identified six putative *Ppargc1a* consensus sites within 1.5 kb of the *ptgs1* open reading frame (Figure 5A) (Charos et al., 2012). Subsequently, we investigated the expression of each gene by WISH and quantitative PCR in reciprocal knockdown studies. The expression of *ppargc1a* was unchanged in *ptgs1* morphants (Figures S5A and S5B). However, the expression of *ptgs1* was decreased in *ppargc1a*-deficient zebrafish (Figures 5B and 5C). These results, in light of the previous rescue experiments, suggested that *ppargc1a* may directly enhance prostaglandin signaling output (Figures 3 and 4). To test this potential relationship, we performed rescue experiments with *ptgs1* capped mRNA injected in *ppargc1a* morphants, then completed IF for cilia and basal bodies or WISH for *odf3b*. We observed a rescue of cilia length, percentage of ciliated basal bodies, and mean fluorescent intensity in both the proximal and distal portions of the pronephros (Figures 5D–5I; Figures S5C and S5D). Also, the number of MCCs present in *ppargc1a* morphants injected with *ptgs1* cRNA was rescued compared with *ppargc1a* morphants (Figures 5J and 5K). Altogether, these data led us to conclude that *ppargc1a* promotes *ptgs1* expression in the pronephros and is needed for proper MCC development and ciliogenesis (Figure 5L).

DISCUSSION

There is broad significance to understanding the genetic mechanisms that control ciliated cell development during embryogenesis. Ciliated cell development involves the distinct processes of fate choice, where for example a cell adopts a monociliated or MCC phenotype, and ciliogenesis, whereby a cell builds the correct number, length, and arrangement of cilia. Although there have been advances in the molecular understanding of ciliated cell development, much remains to be discovered. Recently, prostaglandin signaling was found to be necessary to promote ciliogenesis in numerous vertebrate cell types and during the specification of renal MCCs (Jin et al., 2014; Marra et al., 2019a). However, the genetic mechanisms by which prostaglandin signaling is regulated to perform these tasks were not determined. Here, we found that *ppargc1a* is necessary for ciliogenesis throughout the developing zebrafish and that it also dictates monociliated versus MCC fate choice in the pronephros, in both cases by modulating prostaglandin biosynthesis (Figure 5L). Through a number of experiments, we found that provision of the active prostanoid $dmPGE_2$ rescued *ppargc1a* loss-of-function phenotypes. Furthermore, the results of genetic interaction studies

and rescue experiments nicely complemented our evidence of decreased *ptgs1* RNA and PGE_2 metabolites and led us to determine that *ppargc1a* acts to mitigate *ptgs1* expression that subsequently affects prostanoid levels. These findings unearth fascinating molecular functions of Ppargc1a as a regulator of prostaglandin signaling by exerting control over prostanoid production during ciliated cell development, where a necessary threshold of active prostanoid is essential to control cell fate and cilium growth (Figure 5L). Notably, our studies here also demonstrate that diminished MCC fate and defunct ciliogenesis are not inextricably linked phenotypes, as altered ciliogenesis in *ift88*-deficient embryos occurred simultaneously with normal MCC development in the pronephros. This leads us to conclude that the effects of Ppargc1a/Ptgs1/PGE_2 activity on MCC fate and ciliogenesis are independent outcomes.

Long known for its roles in directing cellular mitochondrial biogenesis and metabolism, PGC-1α can function as a transcription factor but can also interact with chromatin remodeling machinery and RNA processing complexes (Knutti and Kralli, 2001). Interestingly, there has been mounting evidence that PGC-1α is vital to adult kidney health (Lynch et al., 2018). Additionally, although roles for PGC-1α during mammalian development have received comparatively little scrutiny, we found that embryonic kidney formation in the zebrafish is reliant on its ortholog *ppargc1a* (Chambers et al., 2018). In this context, *ppargc1a* is necessary for the proper segmentation of embryonic nephrons via reciprocal antagonism with the essential PST transcription factor Sim1a (Cheng and Wingert, 2015), a genetic interaction that negotiates the caudal boundary of the PST segment (Chambers et al., 2018). The consequence of *ppargc1a* deficiency is that embryos form an expanded PST (Chambers et al., 2018). In the present report we have now elucidated that skewing of tubule fate choice to favor the monociliated cell identity underlies this nephron composition change, where fewer MCC progenitors form in the absence of *ppargc1a*. As other organs contain MCCs, such as the respiratory and reproductive tracts, our findings lay the groundwork for future investigations of *ppargc1a* and prostanoid signaling in these tissue types, which could provide additional insights into MCC pattern formation.

In the context of the adult mammalian kidney, PGC-1α provides renoprotective effects in several injury states including ischemia, toxins or sepsis, where PGC-1α expression promotes the metabolic recovery of nephron tubular cells (Portilla et al., 2002; Tran et al., 2011, 2016; Ruiz-Andres et al., 2016; Lynch et al., 2018). Specifically, in the post-ischemic mouse kidney, it was found that PGC-1α regulates the biosynthesis of nicotinamide adenine dinucleotide (NAD), leading to augmentation of fat catabolism and increased prostaglandin production (Tran et al., 2016). Using the innate ability of the zebrafish to regenerate nephrons post-AKI and tracking the endogenous levels of *ppargc1a* during the regenerative process could help us link essential factors leading to nascent nephrons (Zhou et al., 2010; Diep et al., 2011; McCampbell et al., 2015; McKee and Wingert, 2015). There are also links between PGC-1α and chronic kidney disease, where decreased PGC-1α expression has been found in the human diabetic kidney (Sharma et al., 2013), as well as rat and murine models of diabetic nephropathy (Guo et al., 2015; Long et al., 2016). In these studies, cilium structure and function have not yet been described but would be of great importance to assess given our findings.

Interestingly, PGC-1α expression is also diminished in Pkd1-deficient rodents, a model of polycystic kidney disease (PKD), which has profound cilia defects (Ishimoto et al., 2017). Additionally, PGC-1α levels are directly correlated with *HNF1B* activity in renal cells, and *HNF1B* directly binds to the *ppargc1a* promoter in mouse kidney cells (Casemayou et al., 2017). Mutations in *HNF1B* are known to cause a spectrum of kidney diseases, including PKD, a common ciliopathy (Verhave et al., 2016). In contrast, global or nephron-specific knockout of PGC-1α alone has not yet been linked to changes in renal development or ciliary defects in mice (Lin et al., 2004; Tran et al., 2011; Svensson et al., 2016). However, in light of the present work, this may require further scrutiny. There have been conflicting reports about whether global knockout of PGC-1α results in progeny below the expected Mendelian ratio (Lin et al., 2004; The Jackson Laboratory, 2020), and PGC-1α-knockout pups are more prone to post-natal lethality, heart failure, and neurodegeneration, all facets that might signal the existence of an underlying ciliopathy (Lin et al., 2004; Arany et al., 2006). Alternatively, the functions of PGC-1α in higher vertebrates may not align with Ppargc1a in the zebrafish, despite the high sequence similarity of these orthologs that suggests functional conservation (Chambers et al., 2018).

An additional layer of complexity to fully discerning the roles of PGC-1α during embryogenesis is the relatively recent appreciation that mammals express numerous splice variants of PGC-1α, which exhibit tissue-specific expression patterns and exert different functions (Martínez-Redondo et al., 2015). The existence of these other PGC-1α isoforms could possibly underlie the absence of more severe phenotypes in murine knockout animals that survive the post-natal period, because the floxed region does not target some of the variants identified to date (Lin et al., 2004; Tran et al., 2011, 2016; Svensson et al., 2016; Zerbino et al., 2018). Furthermore, the nephron-specific PGC-1α conditional knockout mice exhibited significantly reduced, but not abrogated, expression of PGC-1α transcripts and therefore likely represent a hypomorphic loss-of-function model (Svensson et al., 2016). Future efforts to exhaustively isolate and characterize variants of PGC-1α are needed to assess whether there are functional isoforms that are essential to renal lineage ontogeny in mammals.

Other intriguing directions include elucidating the relationship between *ppargc1a* with other factors that control MCC fate and ciliogenesis. Previous research has found that *ptgs2*, which encodes the cyclooxygenase Cox2, is also important for MCC specification and ciliogenesis during MCC maturation (Marra et al., 2019a). This study did not reveal a significant difference in MCC development when comparing loss of *ptgs1* with loss of *ptgs2*. However, further research could be completed to identify if *ptgs2* expression is also affected by *ppargc1a* expression or if it acts in a compensatory manner when *ppargc1a* and *ptgs1* are absent. Other options such as CaMK-II and histone deacetylases (HDACs), which were recently shown to have a role in zebrafish ciliogenesis, present possible avenues of exploration (Rothschild et al., 2018). Furthermore, future studies to explore the relationship of *ppargc1a*/prostanoid signaling with requisite MCC regulators such as Notch signaling, transcription factors (such as *mecom*, *etv5a*, *irx2a*, and *e2f5*), and ciliogenesis regulators (such as *foxj1*) have merit as well (Deblandre et al., 1999; Hellman et al., 2010; Li et al., 2014; Liu et al., 2007; Ma and Jiang, 2007; Marra et al., 2016, 2019b; Tsao et al., 2009; Xie et al., 2020).

In conclusion, in this work we have determined essential functions of *ppargc1a* in ciliated cell development in the zebrafish, identifying *ppargc1a* as a key regulator of prostaglandin synthesis through its control of *ptgs1* expression. These results may be relevant for understanding the mechanisms of ciliated cell formation across tissues given the pleiotropic cilia defects that occur in *ppargc1a* zebrafish mutant embryos. Furthermore, considering the human disease burden related to ciliary defects, these findings may suggest PGC-1α as a target of interest for therapeutic applications.

STAR⋆METHODS

RESOURCE AVAILABILITY

Lead Contact—Further information and requests for resources and reagents should be directed to and will be fulfilled by the Lead Contact, Rebecca A. Wingert (rwingert@nd.edu).

Materials Availability—This study did not generate any unique reagents. The zebrafish *ppargc1a* ^{sa13186} mutant line is distributed by the Zebrafish International Resource Center.

Data and Code Availability—All used software is listed in the Key Resources Table. This study did not generate any unique datasets or new code.

EXPERIMENTAL MODEL AND SUBJECT DETAILS

The Center for Zebrafish Research at the University of Notre Dame maintained the zebrafish used in these studies and experiments were performed with approval of the University of Notre Dame Institutional Animal Care and Use Committee (IACUC), under protocol numbers 16–07-3245 and 19–06-5412.

Animal models—Tübingen strain zebrafish were used for all studies, with the *ppargc1a*^{sa13186} mutation propagated on this background. Zebrafish were raised and staged as described (Kimmel et al., 1995). For all studies, embryos were incubated in E3 medium at 28°C until the desired developmental stage, anesthetized with 0.02% tricaine, and then fixed using 4% paraformaldehyde/1x PBS (PFA) (Westerfield, 1993). Embryos were analyzed before sex determination, so the influence of gender cannot be reported in the context of this study.

METHOD DETAILS

Whole mount and fluorescent whole mount *in situ* hybridization (WISH, FISH)—WISH was performed as previously described (Cheng et al., 2014; Galloway et al., 2008; Lengerke et al., 2011; Marra et al., 2019c) with antisense RNA probes either digoxigenin-labeled (*ppargc1a, odf3b, slc20a1a, trpm7, jag2b, myl7, ptgs1*) or fluorescein-labeled (*odf3b*) via *in vitro* transcription using IMAGE clone templates as previously described (Wingert et al., 2007; O'Brien et al., 2011; Gerlach and Wingert, 2014). FISH was performed as described (Brend and Holley 2009; Marra et al., 2017) using TSA Plus Fluorescein or Cyanine Kits (Akoya Biosciences). For all gene expression studies, every

analysis was done in triplicate for each genetic model, and measurements were scored in a blinded fashion, with sample sizes of n > 20 per replicate.

Sectioning—Zebrafish were embedded for JB4 sectioning and counterstained as previously described (Gerlach and Wingert, 2014).

Dextran-FITC injections—*ppargc1a*^{sa13186} heterozygous incrosses were incubated in 0.003% phenylthiourea (Sigma, P7629) in E3 from 24 hpf until 48 hpf. Zebrafish were anesthetized in 0.02% tricaine and microinjected was performed directly into the circulation as described (Kroeger et al., 2017) at the 48 hpf time point with 5 mg/ml 40 kDa dextran-FITC (Invitrogen, D1845). Embryos were again incubated in 0.003% PTU until 72 hpf when they were imaged.

Immunofluorescence (IF)—Whole mount IF experiments were completed as previously described (Gerlach and Wingert, 2014; Kroeger et al., 2017; Marra et al., 2017, 2019c). For cilia and basal bodies, anti-tubulin acetylated diluted 1:400 (Sigma T6793) and anti γ-tubulin diluted 1:400 (Sigma T5192) were used, respectively. The anti-Ppargc1a was diluted 1:150 (Abcam, AB54481) (Ran et al., 2017, Blechman et al., 2011), and anti-PKC was diluted 1:500 (Santa Cruz, SC216). Anti-rabbit and anti-mouse secondary antibodies were diluted 1:500 (Alexa Fluor, Invitrogen).

Rescue Experiments with dmPGE$_2$—Chemical treatments were completed as previously described (Marra et al., 2019a; Poureetezadi et al., 2014; Poureetezadi et al., 2016). 16,16-Dimethyl-prostaglandin E2 (Santa Cruz Biotechnology, Inc, SC-201240) was dissolved in 100% dimethyl sulfoxide (DMSO) to make 1 M stocks then diluted to the 100 μM treatment dose. Treatments were completed in triplicate with n > 20 embryos per replicate.

PGE$_2$ metabolite quantification—PGE$_2$ metabolite quantifications were completed according to the manufacturer's protocol (Cayman Chemical #500141). In brief, groups of 50 WT or *ppargc1a* MO injected zebrafish were pooled, anesthetized, and flash frozen in 100% ethanol. Lysates were homogenized and supernatant was isolated after centrifugation at 4 degrees (12,000 RPM for 10 minutes). Kit reagents were used to complete plate set up and manufacturer's protocol was followed for assay completion using a plate reader (SpectraMax ABSPlus) at 420 nm.

Quantitative real-time PCR—Groups of 30 zebrafish (WT, *ppargc1a* morphants, or *ptgs1* morphants) were pooled at 24 hpf. Trizol (Ambion) was used to extract RNA, qScript cDNA SuperMix (QuantaBio) was used to make cDNA. PerfeCTa SYBR Green SuperMix with ROX (QuantaBio) was used to complete qRT-PCR with 100 ng for *ptgs1* and *ppargc1a* and 1 ng for 18S controls being optimal cDNA concentrations. The AB StepOnePlus qRT-PCR machine was used with the following program: 2 minute 50°C hold, 10 minute 95°C hold, then 35 cycles of 15 s at 95°C and 1 minute at 60°C for denaturing and primer annealing and product extension steps respectively. Each target and source were completed in biological replicates and technical replicates each with the median Ct value normalized to the control. Data analysis was completed by using delta delta Ct values comparing WT

uninjected to the respective morphant groups with 18S as a reference. Primers used include: *ppargc1a* forward 5′–AATGCCAGTGATCAGAGCTGTCCTT–3′ and reverse 5′–GTTCTGTGCCTTGCCACCTGGGTAT–3′. To target 18S: forward 5′–TCGGCTACCACATCCAAGGAAGGCAGC–3′ and reverse 5′–TTGCTGGAATTACCGCGGCTGCTGGCA–3′. To target *ptgs1*: forward 5′-CATGCACAGGTCAAAATGAGTT- 3′ reverse: 5′-TGTGAGGATCGATGTGTTGAAT-3′.

Genetic models—The *ppargc1a*^{sa13186} line (*ppargc1a*$^{sa13186/sa13186}$) was obtained from ZIRC (Eugene, OR) (Busch-Nentwich et al., 2013). Homozygous mutant and heterozygous zebrafish were identified as previously described (Chambers et al., 2018) using genotyping primers, forward 5′–GGGCCGGCATGTGGAATGTAAAGACTTAAACATGCCAACCTCCACTACTACGACA TCATCGTTGTCTTCCACCCCCCC TTCGTCTTCCTCACTGGCCAGG–3′, and reverse 5′–TCCCACTACCCCGCTATAGAAGGCTTGCTGAGGCTTTCCAAAGTGCTTGTTGAGCT CGTCCCGGATCTCCTGGTCCCTAAGAAGTTTCCTGCCACCAGAA–3′. Antisense morpholino oligonucleotides (MOs) were obtained from Gene Tools, LLC (Philomath, OR). MOs were solubilized in DNase/RNase free water to generate 4 mM stock solutions which were stored at −20°C. Zebrafish embryos were injected at the 1-cell stage with 1–2 nL of diluted MO. *ppargc1a* was targeted with the following validated MO: 5′–CCTGATTACACCTGTCCCACGCCAT–3′ (400 μM optimal, 200 μM suboptimal) (Hanai et al., 2007; Bertrand et al., 2007, Chambers et al., 2018). *ptgs1* was targeted with the following validated MO: 5′-TCAGCAAAAAGTTACACTCTCTCAT-3′ (400 μM optimal, 200 μM suboptimal) (Marra et al., 2019a; Poureetezadi et al., 2016, North et al., 2007). The *ift88* MO was 5′-AGCAGATGCAAAATGACTCACTGGG-3′ (100uM) (Vasilyev et al., 2009; Gerlach and Wingert, 2014). Control MO was 5′-CCTCTTACCTCAGTTACAATTTATA-3′ (400uM) (Gene Tools, LLC).

Image acquisition and phenotype quantification—A Nikon Eclipse Ni with a DS-Fi2 camera was used to image WISH samples and live zebrafish. Live zebrafish were mounted in methyl cellulose with trace amounts of tricaine present. IF and FISH images were acquired using a Nikon C2 confocal microscope.

QUANTIFICATION AND STATISTICAL ANALYSIS

Cilia phenotypes were quantified using ImageJ/Fiji (https://imagej.nih.gov) software tools. All measurements were completed on representative samples imaged at 60X magnification. The multi-point tool was used for counting. The segmented line tool was used for length measurements. Fluorescent intensity plots were generated with the plot profile function. Each experiment was completed in triplicate. From these measurements an average and standard deviation (SD) were calculated, and unpaired t tests or one-way ANOVA tests were completed to compare control and experimental measurements using GraphPad Prism 8 software. Statistical details for each experiment are located in the figure legends.

Supplementary Material

Refer to Web version on PubMed Central for supplementary material.

ACKNOWLEDGMENTS

We thank the staffs of the Department of Biological Sciences for support and the Center for Zebrafish Research at the University of Notre Dame for outstanding care of our zebrafish aquarium. We thank the members of our lab for discussions and insights about this work. This work was supported in part by the National Institutes of Health (R01DK100237 to R.A.W.), a 2019 University of Notre Dame Advanced Diagnostics and Therapeutics Graduate Fellowship Award (to J.M.C.), a 2019 University of Notre Dame College of Science Summer Undergraduate Research Fellowship Award (to A.A.), and laboratory start-up funds from the University of Notre Dame (to A.L.F.-M. and R.A.W.). We are grateful to Elizabeth and Michael Gallagher for a generous gift to the University of Notre Dame for the support of stem cell research. The funders had no role in the study design, data collection and analysis, decision to publish, or manuscript preparation.

REFERENCES

Arany Z, Novikov M, Chin S, Ma Y, Rosenzweig A, and Spiegelman BM (2006). Transverse aortic constriction leads to accelerated heart failure in mice lacking PPAR-g coactivator 1a. Proc. Natl. Acad. Sci. U S A 103, 10086–10091. [PubMed: 16775082]

Bertrand S, Thisse B, Tavares R, Sachs L, Chaumot A, Bardet PL, Escrivá H, Duffraisse M, Marchand O, Safi R, et al. (2007). Unexpected novel relational links uncovered by extensive developmental profiling of nuclear receptor expression. PLoS Genet 3, e188. [PubMed: 17997606]

Bisgrove BW, Snarr BS, Emrazian A, and Yost HJ (2005). Polaris and Polycystin-2 in dorsal forerunner cells and Kupffer's vesicle are required for specification of the zebrafish left-right axis. Dev. Biol 287, 274–288. [PubMed: 16216239]

Blechman J, Amir-Zilberstein L, Gutnick A, Ben-Dor S, and Levkowitz G (2011). The metabolic regulator PGC-1α directly controls the expression of the hypothalamic neuropeptide oxytocin. J. Neurosci 31, 14835–14840. [PubMed: 22016516]

Brend T, and Holley SA (2009). Zebrafish whole mount high-resolution double fluorescent in situ hybridization. J. Vis. Exp 25, e1229.

Busch-Nentwich E, Kettleborough R, Dooley CM, Scahill C, Sealy I, White R, Herd C, Mehroke S, Wali N, Carruthers S, et al. (2013). Sanger Institute Zebrafish Mutation Project mutant data submission. ZFIN Direct Data Submission. http://zfin.org/ZDB-PUB-130425-4.

Casemayou A, Fournel A, Bagattin A, Schanstra J, Belliere J, Decramer S, Marsal D, Gillet M, Chassaing N, Huart A, et al. (2017). Hepatocyte nuclear factor-1β controls mitochondrial respiration in renal tubular cells. J. Am. Soc. Nephrol 28, 3205–3217. [PubMed: 28739648]

Chambers JM, and Wingert RA (2020). PGC-1α in disease: recent renal insights into a versatile metabolic regulator. Cells 9, 2234.

Chambers JM, Poureetezadi SJ, Addiego A, Lahne M, and Wingert RA (2018). *ppargc1a* controls nephron segmentation during zebrafish embryonic kidney ontogeny. eLife 7, e40266. [PubMed: 30475208]

Charos AE, Reed BD, Raha D, Szekely AM, Weissman SM, and Snyder M (2012). A highly integrated and complex PPARGC1A transcription factor binding network in HepG2 cells. Genome Res 22, 1668–1679. [PubMed: 22955979]

Cheng CN, and Wingert RA (2015). Nephron proximal tubule patterning and corpuscles of Stannius formation are regulated by the sim1a transcription factor and retinoic acid in zebrafish. Dev. Biol 399, 100–116. [PubMed: 25542995]

Cheng CN, Li Y, Marra AN, Verdun V, and Wingert RA (2014). Flat mount preparation for observation and analysis of zebrafish embryo specimens stained by whole mount in situ hybridization. J. Vis. Exp 89, 51604.

Choi SY, Baek JI, Zuo X, Kim SH, Dunaief JL, and Lipschutz JH (2015). Cdc42 and sec10 are required for normal retinal development in zebrafish. Invest. Ophthalmol. Vis. Sci 56, 3361–3370. [PubMed: 26024121]

Compagnon J, Barone V, Rajshekar S, Kottmeier R, Pranjic-Ferscha K, Behrndt M, and Heisenberg CP (2014). The notochord breaks bilateral symmetry by controlling cell shapes in the zebrafish laterality organ. Dev. Cell 31, 774–783. [PubMed: 25535919]

Dasgupta A, and Amack JD (2016). Cilia in vertebrate left-right patterning. Philos. Trans. R. Soc. Lond. B Biol. Sci 371, 20150410. [PubMed: 27821522]

Deblandre GA, Wettstein DA, Koyano-Nakagawa N, and Kintner C (1999). A two-step mechanism generates the spacing pattern of the ciliated cells in the skin of Xenopus embryos. Development 126, 4715–4728. [PubMed: 10518489]

DiBella LM, Park A, and Sun Z (2009). Zebrafish Tsc1 reveals functional interactions between the cilium and the TOR pathway. Hum. Mol. Genet 18, 595–606. [PubMed: 19008302]

Diep CQ, Ma D, Deo RC, Holm TM, Naylor RW, Arora N, Wingert RA, Bollig F, Djordjevic G, Lichman B, et al. (2011). Identification of adult nephron progenitors capable of kidney regeneration in zebrafish. Nature 470, 95–100. [PubMed: 21270795]

Drummond IA, Majumdar A, Hentschel H, Elger M, Solnica-Krezel L, Schier AF, Neuhauss SC, Stemple DL, Zwartkruis F, Rangini Z, et al. (1998). Early development of the zebrafish pronephros and analysis of mutations affecting pronephric function. Development 125, 4655–4667. [PubMed: 9806915]

Esain V, Kwan W, Carroll KJ, Cortes M, Liu SY, Frechette GM, Sheward LM, Nissim S, Goessling W, and North TE (2015). Cannabinoid receptor-2 regulates embryonic hematopoietic stem cell development via prostaglandin E2 and p-selectin activity. Stem Cells 33, 2596–2612. [PubMed: 25931248]

Essner JJ, Vogan KJ, Wagner MK, Tabin CJ, Yost HJ, and Brueckner M (2002). Conserved function for embryonic nodal cilia. Nature 418, 37–38. [PubMed: 12097899]

Essner JJ, Amack JD, Nyholm MK, Harris EB, and Yost HJ (2005). Kupffer's vesicle is a ciliated organ of asymmetry in the zebrafish embryo that initiates left-right development of the brain, heart and gut. Development 132, 1247–1260. [PubMed: 15716348]

Fliegauf M, Benzing T, and Omran H (2007). When cilia go bad: cilia defects and ciliopathies. Nat. Rev. Mol. Cell Biol 8, 880–893. [PubMed: 17955020]

Galloway JL, Wingert RA, Thisse C, Thisse B, and Zon LI (2008). Combinatorial regulation of novel erythroid gene expression in zebrafish. Exp. Hematol 36, 424–432. [PubMed: 18243489]

Gerlach GF, and Wingert RA (2014). Zebrafish pronephros tubulogenesis and epithelial identity maintenance are reliant on the polarity proteins Prkc iota and zeta. Dev. Biol 396, 183–200. [PubMed: 25446529]

Guo K, Lu J, Huang Y, Wu M, Zhang L, Yu H, Zhang M, Bao Y, He JC, Chen H, and Jia W (2015). Protective role of PGC-1α in diabetic nephropathy is associated with the inhibition of ROS through mitochondrial dynamic remodeling. PLoS ONE 10, e0125176. [PubMed: 25853493]

Hanai J, Cao P, Tanksale P, Imamura S, Koshimizu E, Zhao J, Kishi S, Yamashita M, Phillips PS, Sukhatme VP, and Lecker SH (2007). The muscle-specific ubiquitin ligase atrogin-1/MAFbx mediates statin-induced muscle toxicity. J. Clin. Invest 117, 3940–3951. [PubMed: 17992259]

Hellman NE, Liu Y, Merkel E, Austin C, Le Corre S, Beier DR, Sun Z, Sharma N, Yoder BK, and Drummond IA (2010). The zebrafish foxj1a transcription factor regulates cilia function in response to injury and epithelial stretch. Proc. Natl. Acad. Sci. U S A 107, 18499–18504. [PubMed: 20937855]

Huang S, Ma J, Liu X, Zhang Y, and Luo L (2011). Retinoic acid signaling sequentially controls visceral and heart laterality in zebrafish. J. Biol. Chem 286, 28533–28543. [PubMed: 21669875]

Ishimoto Y, Inagi R, Yoshihara D, Kugita M, Nagao S, Shimizu A, Takeda N, Wake M, Honda K, Zhou J, and Nangaku M (2017). Mitochondrial abnormality facilitates cyst formation in autosomal dominant polycystic kidney disease. Mol. Cell. Biol 37, e00337–17. [PubMed: 28993480]

The Jackson Laboratory (2020). B6.129S4(FVB)-Ppargc1atm1Brsp/J strain detail.https://www.informatics.jax.org/strain/MGI:3842631.

Jin D, Ni TT, Sun J, Wan H, Amack JD, Yu G, Fleming J, Chiang C, Li W, Papierniak A, et al. (2014). Prostaglandin signalling regulates ciliogenesis by modulating intraflagellar transport. Nat. Cell Biol 16, 841–851. [PubMed: 25173977]

Kallakuri S, Yu JA, Li J, Li Y, Weinstein BM, Nicoli S, and Sun Z (2015). Endothelial cilia are essential for developmental vascular integrity in zebrafish. J. Am. Soc. Nephrol 26, 864–875. [PubMed: 25214579]

Kimmel CB, Ballard WW, Kimmel SR, Ullmann B, and Schilling TF (1995). Stages of embryonic development of the zebrafish. Dev. Dyn 203, 253–310. [PubMed: 8589427]

Knutti D, and Kralli A (2001). PGC-1, a versatile coactivator. Trends Endocrinol. Metab 12, 360–365. [PubMed: 11551810]

Kramer-Zucker AG, Olale F, Haycraft CJ, Yoder BK, Schier AF, and Drummond IA (2005). Cilia-driven fluid flow in the zebrafish pronephros, brain and Kupffer's vesicle is required for normal organogenesis. Development 132, 1907–1921. [PubMed: 15790966]

Kroeger PT Jr., Drummond BE, Miceli R, McKernan M, Gerlach GF, Marra AN, Fox A, McCampbell KK, Leshchiner I, Rodriguez-Mari A, et al. (2017). The zebrafish kidney mutant zeppelin reveals that brca2/fancd1 is essential for pronephros development. Dev. Biol 428, 148–163. [PubMed: 28579318]

Lengerke C, Wingert R, Beeretz M, Grauer M, Schmidt AG, Konantz M, Daley GQ, and Davidson AJ (2011). Interactions between Cdx genes and retinoic acid modulate early cardiogenesis. Dev. Biol 354, 134–142. [PubMed: 21466798]

Li Y, Cheng CN, Verdun VA, and Wingert RA (2014). Zebrafish nephrogenesis is regulated by interactions between retinoic acid, mecom, and Notch signaling. Dev. Biol 386, 111–122. [PubMed: 24309209]

Lin J, Wu PH, Tarr PT, Lindenberg KS, St-Pierre J, Zhang CY, Mootha VK, Jäger S, Vianna CR, Reznick RM, et al. (2004). Defects in adaptive energy metabolism with CNS-linked hyperactivity in PGC-1α null mice. Cell 119, 121–135. [PubMed: 15454086]

Liu Y, Pathak N, Kramer-Zucker A, and Drummond IA (2007). Notch signaling controls the differentiation of transporting epithelia and multiciliated cells in the zebrafish pronephros. Development 134, 1111–1122. [PubMed: 17287248]

Long J, Badal SS, Ye Z, Wang Y, Ayanga BA, Galvan DL, Green NH, Chang BH, Overbeek PA, and Danesh FR (2016). Long noncoding RNA Tug1 regulates mitochondrial bioenergetics in diabetic nephropathy. J. Clin. Invest 126, 4205–4218. [PubMed: 27760051]

Lynch MR, Tran MT, and Parikh SM (2018). PGC1α in the kidney. Am. J. Physiol. Renal Physiol 314, F1–F8. [PubMed: 28931521]

Ma M, and Jiang YJ (2007). Jagged2a-notch signaling mediates cell fate choice in the zebrafish pronephric duct. PLoS Genet 3, e18. [PubMed: 17257056]

Manning DK, Sergeev M, van Heesbeen RG, Wong MD, Oh JH, Liu Y, Henkelman RM, Drummond I, Shah JV, and Beier DR (2013). Loss of the ciliary kinase Nek8 causes left-right asymmetry defects. J. Am. Soc. Nephrol 24, 100–112. [PubMed: 23274954]

Marra AN, and Wingert RA (2016). Epithelial cell fate in the nephron tubule is mediated by the ETS transcription factors etv5a and etv4 during zebrafish kidney development. Dev. Biol 411, 231–245. [PubMed: 26827902]

Marra AN, Li Y, and Wingert RA (2016). Antennas of organ morphogenesis: the roles of cilia in vertebrate kidney development. Genesis 54, 457–469. [PubMed: 27389733]

Marra AN, Ulrich M, White A, Springer M, and Wingert RA (2017). Visualizing multiciliated cells in the zebrafish through a combined protocol of whole mount fluorescent in situ hybridization and immunofluorescence. J. Vis. Exp 129, e56261.

Marra AN, Adeeb BD, Chambers BE, Drummond BE, Ulrich M, Addiego A, Springer M, Poureetezadi SJ, Chambers JM, Ronshaugen M, and Wingert RA (2019a). Prostaglandin signaling regulates renal multiciliated cell specification and maturation. Proc. Natl. Acad. Sci. U S A 116, 8409–8418. [PubMed: 30948642]

Marra AN, Cheng CN, Adeeb B, Addiego A, Wesselman HM, Chambers BE, Chambers JM, and Wingert RA (2019b). Iroquois transcription factor irx2a is required for multiciliated and transporter cell fate decisions during zebrafish pronephros development. Sci. Rep. 9, 6454. [PubMed: 31015532]

Marra AN, Chambers BE, Chambers JM, Drummond BE, Adeeb BD, Wesselman HM, Morales EE, Handa N, Pettini T, Ronshaugen M, and Wingert RA (2019c). Visualizing gene expression during

zebrafish pronephros development and regeneration. Methods Cell Biol 154, 183–215. [PubMed: 31493818]

Martínez-Redondo V, Pettersson AT, and Ruas JL (2015). The hitchhiker's guide to PGC-1α isoform structure and biological functions. Diabetologia 58, 1969–1977. [PubMed: 26109214]

McCampbell KK, Springer KN, and Wingert RA (2015). Atlas of cellular dynamics during zebrafish adult kidney regeneration. Stem Cells Int 2015, 547636. [PubMed: 26089919]

McKee RA, and Wingert RA (2015). Zebrafish renal pathology: emerging models of acute kidney injury. Curr. Pathobiol. Rep 3, 171–181. [PubMed: 25973344]

Mitchison HM, and Valente EM (2017). Motile and non-motile cilia in human pathology: from function to phenotypes. J. Pathol 241, 294–309. [PubMed: 27859258]

Moyer JH, Lee-Tischler MJ, Kwon HY, Schrick JJ, Avner ED, Sweeney WE, Godfrey VL, Cacheiro NL, Wilkinson JE, and Woychik RP (1994). Candidate gene associated with a mutation causing recessive polycystic kidney disease in mice. Science 264, 1329–1333. [PubMed: 8191288]

North TE, Goessling W, Walkley CR, Lengerke C, Kopani KR, Lord AM, Weber GJ, Bowman TV, Jang IH, Grosser T, et al. (2007). Prostaglandin E2 regulates vertebrate haematopoietic stem cell homeostasis. Nature 447, 1007–1011. [PubMed: 17581586]

O'Brien LL, Grimaldi M, Kostun Z, Wingert RA, Selleck R, and Davidson AJ (2011). Wt1a, Foxc1a, and the Notch mediator Rbpj physically interact and regulate the formation of podocytes in zebrafish. Dev. Biol 358, 318–330. [PubMed: 21871448]

Portilla D, Dai G, McClure T, Bates L, Kurten R, Megyesi J, Price P, and Li S (2002). Alterations of PPARalpha and its coactivator PGC-1 in cisplatin-induced acute renal failure. Kidney Int 62, 1208–1218. [PubMed: 12234291]

Poureetezadi SJ, Donahue EK, and Wingert RA (2014). A manual small molecule screen approaching high-throughput using zebrafish embryos. J. Vis. Exp 93, e52063.

Poureetezadi SJ, Cheng CN, Chambers JM, Drummond BE, and Wingert RA (2016). Prostaglandin signaling regulates nephron segment patterning of renal progenitors during zebrafish kidney development. eLife 5, e17551. [PubMed: 27996936]

Puigserver P, and Spiegelman BM (2003). Peroxisome proliferator-activated receptor-gamma coactivator 1 alpha (PGC-1 alpha): transcriptional coactivator and metabolic regulator. Endocr. Rev 24, 78–90. [PubMed: 12588810]

Ran G, Ying L, Li L, Yan Q, Yi W, Ying C, Wu H, and Ye X (2017). Resveratrol ameliorates diet-induced dysregulation of lipid metabolism in zebrafish (Danio rerio). PLoS ONE 12, e0180865. [PubMed: 28686680]

Reiter JF, and Leroux MR (2017). Genes and molecular pathways underpinning ciliopathies. Nat. Rev. Mol. Cell Biol 18, 533–547. [PubMed: 28698599]

Rothschild SC, Lee HJ, Ingram SR, Mohammadi DK, Walsh GS, and Tombes RM (2018). Calcium signals act through histone deacetylase to mediate pronephric kidney morphogenesis. Dev. Dyn. 247, 807–817. [PubMed: 29633426]

Ruiz-Andres O, Suarez-Alvarez B, Sánchez-Ramos C, Monsalve M, Sanchez-Niño MD, Ruiz-Ortega M, Egido J, Ortiz A, and Sanz AB (2016). The inflammatory cytokine TWEAK decreases PGC-1α expression and mitochondrial function in acute kidney injury. Kidney Int. 89, 399–410. [PubMed: 26535995]

Sharma K, Karl B, Mathew AV, Gangoiti JA, Wassel CL, Saito R, Pu M, Sharma S, You YH, Wang L, et al. (2013). Metabolomics reveals signature of mitochondrial dysfunction in diabetic kidney disease. J. Am. Soc. Nephrol 24, 1901–1912. [PubMed: 23949796]

Stooke-Vaughan GA, Huang P, Hammond KL, Schier AF, and Whitfield TT (2012). The role of hair cells, cilia and ciliary motility in otolith formation in the zebrafish otic vesicle. Development 139, 1777–1787. [PubMed: 22461562]

Sullivan-Brown J, Schottenfeld J, Okabe N, Hostetter CL, Serluca FC, Thiberge SY, and Burdine RD (2008). Zebrafish mutations affecting cilia motility share similar cystic phenotypes and suggest a mechanism of cyst formation that differs from pkd2 morphants. Dev. Biol 314, 261–275. [PubMed: 18178183]

Sun Z, Amsterdam A, Pazour GJ, Cole DG, Miller MS, and Hopkins N (2004). A genetic screen in zebrafish identifies cilia genes as a principal cause of cystic kidney. Development 131, 4085–4093. [PubMed: 15269167]

Svensson K, Schnyder S, Cardel B, and Handschin C (2016). Loss of renal tubular PGC-1α exacerbates diet-induced renal steatosis and age-related urinary sodium excretion in mice. PLoS ONE 11, e0158716. [PubMed: 27463191]

Tian T, Zhao L, Zhang M, Zhao X, and Meng A (2009). Both foxj1a and foxj1b are implicated in left-right asymmetric development in zebrafish embryos. Biochem. Biophys. Res. Commun 380, 537–542. [PubMed: 19284996]

Tran M, Tam D, Bardia A, Bhasin M, Rowe GC, Kher A, Zsengeller ZK, Akhavan-Sharif MR, Khankin EV, Saintgeniez M, et al. (2011). PGC-1α promotes recovery after acute kidney injury during systemic inflammation in mice. J. Clin. Invest 121, 4003–4014. [PubMed: 21881206]

Tran MT, Zsengeller ZK, Berg AH, Khankin EV, Bhasin MK, Kim W, Clish CB, Stillman IE, Karumanchi SA, Rhee EP, and Parikh SM (2016). PGC1α drives NAD biosynthesis linking oxidative metabolism to renal protection. Nature 531, 528–532. [PubMed: 26982719]

Tsao PN, Vasconcelos M, Izvolsky KI, Qian J, Lu J, and Cardoso WV (2009). Notch signaling controls the balance of ciliated and secretory cell fates in developing airways. Development 136, 2297–2307. [PubMed: 19502490]

Vasilyev A, Liu Y, Mudumana S, Mangos S, Lam PY, Majumdar A, Zhao J, Poon KL, Kondrychyn I, Korzh V, and Drummond IA (2009). Collective cell migration drives morphogenesis of the kidney nephron. PLoS Biol 7, e9. [PubMed: 19127979]

Verhave JC, Bech AP, Wetzels JF, and Nijenhuis T (2016). Hepatocyte nuclear factor 1β–associated kidney disease: more than renal cysts and diabetes. J. Am. Soc. Nephrol 27, 345–353. [PubMed: 26319241]

Wagle M, Mathur P, and Guo S (2011). Corticotropin-releasing factor critical for zebrafish camouflage behavior is regulated by light and sensitive to ethanol. J. Neurosci 31, 214–224. [PubMed: 21209207]

Wang G, Cadwallader AB, Jang DS, Tsang M, Yost HJ, and Amack JD (2011). The Rho kinase Rock2b establishes anteroposterior asymmetry of the ciliated Kupffer's vesicle in zebrafish. Development 138, 45–54. [PubMed: 21098560]

Wang G, Manning ML, and Amack JD (2012). Regional cell shape changes control form and function of Kupffer's vesicle in the zebrafish embryo. Dev. Biol 370, 52–62. [PubMed: 22841644]

Westerfield M (1993). The Zebrafish Book (Eugene: University of Oregon Press).

Wingert RA, Selleck R, Yu J, Song HD, Chen Z, Song A, Zhou Y, Thisse B, Thisse C, McMahon AP, and Davidson AJ (2007). The cdx genes and retinoic acid control the positioning and segmentation of the zebrafish pronephros. PLoS Genet 3, 1922–1938. [PubMed: 17953490]

Wu D, Freund JB, Fraser SE, and Vermot J (2011). Mechanistic basis of otolith formation during teleost inner ear development. Dev. Cell 20, 271–278. [PubMed: 21316594]

Xie H, Kang Y, Wang S, Zheng P, Chen Z, Roy S, and Zhao C (2020). E2f5 is a versatile transcriptional activator required for spermatogenesis and multiciliated cell differentiation in zebrafish. PLoS Genet 16, e1008655. [PubMed: 32196499]

Yoder BK, Richards WG, Sweeney WE, Wilkinson JE, Avener ED, and Woychik RP (1995). Insertional mutagenesis and molecular analysis of a new gene associated with polycystic kidney disease. Proc. Assoc. Am. Physicians 107, 314–323. [PubMed: 8608416]

Yu X, Lau D, Ng CP, and Roy S (2011). Cilia-driven fluid flow as an epigenetic cue for otolith biomineralization on sensory hair cells of the inner ear. Development 138, 487–494. [PubMed: 21205793]

Zerbino DR, Achuthan P, Akanni W, Amode MR, Barrell D, Bhai J, Billis K, Cummins C, Gall A, Girón CG, et al. (2018). Ensembl 2018. Nucleic Acids Res 46 (D1), D754–D761. [PubMed: 29155950]

Zhou W, Boucher RC, Bollig F, Englert C, and Hildebrandt F (2010). Characterization of mesonephric development and regeneration using transgenic zebrafish. Am. J. Physiol. Renal Physiol 299, F1040–F1047. [PubMed: 20810610]

Highlights

- *ppargc1a* is required for ciliogenesis in nodal, mono-, and multiciliated cells
- *ppargc1a* mitigates renal tubule ciliated cell fate discernment during embryogenesis
- Ppargc1a controls PGE_2 production through the prostanoid biosynthesis gene *ptgs1*

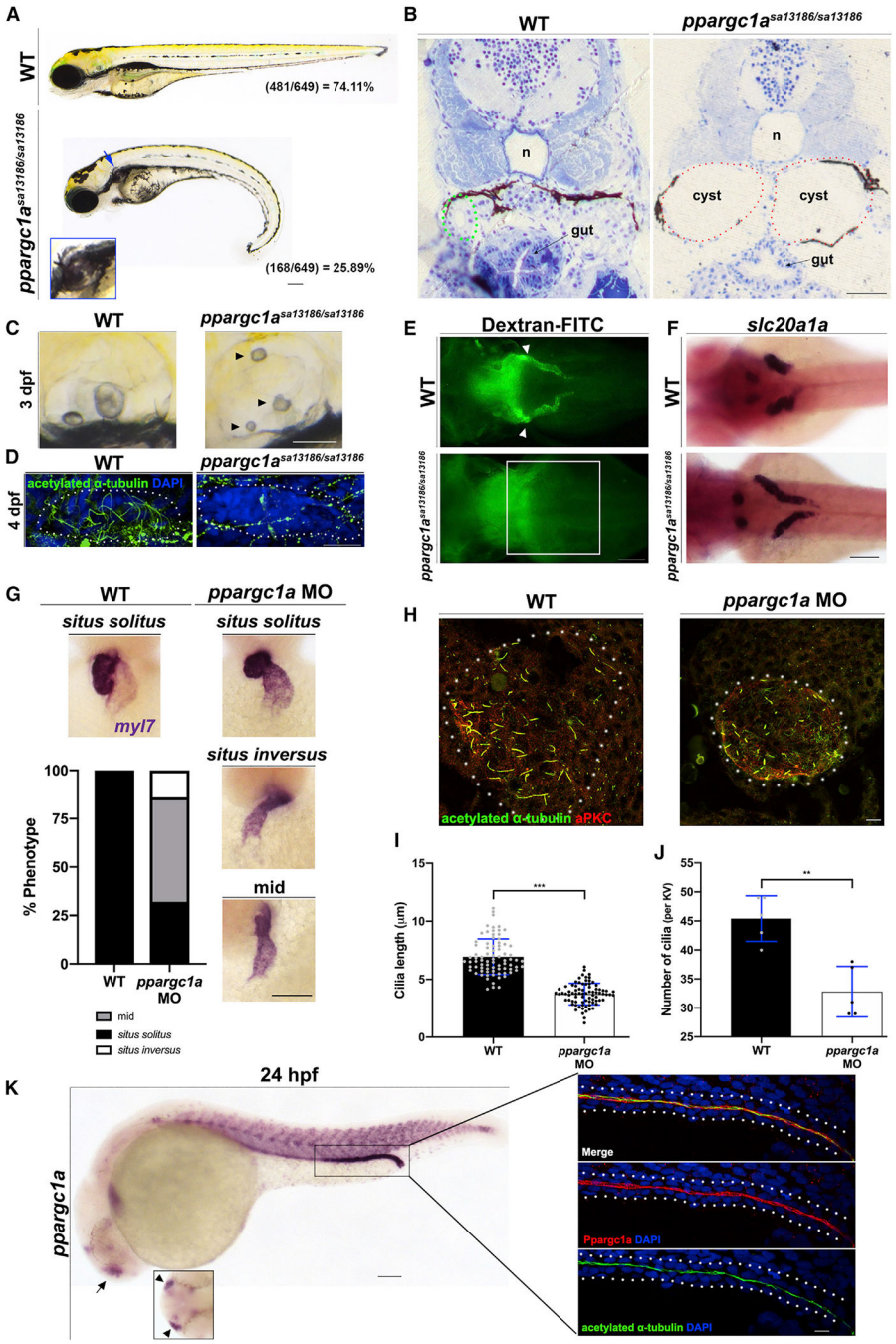

Figure 1. *ppargc1a*-Deficient Zebrafish Display Phenotypes Commonly Associated with Cilia Defects

(A) WT sibling (top) and a *ppargc1a*$^{sa13186/13186}$ mutant (bottom) zebrafish with a curly tail, pronephric cyst (blue arrow, inset), and pericardial edema at 3 dpf. Heterozygous crosses resulted in the expected Mendelian ratio shown at the bottom right of the respective panels (WT group includes homozygous WT and *ppargc1a*$^{+/sa13186}$ combined). Scale bar, 90 μm. (B) JB4 transverse section of a 4 dpf WT sibling (left) and *ppargc1a*$^{sa13186/sa13186}$ mutant (right) zebrafish (n, notochord; tubule outlined in green, cysts outlined in red). Scale bar, 90 μm.

(C) Three days post-fertilization WT sibling (left) and *ppargc1a*$^{sa13186/sa13186}$ mutant (right) otoliths. Arrowheads indicate abnormal otoliths present in the mutant. Scale bar, 90 μm.
(D) Four days post-fertilization otic cilia (green, acetylated α-tubulin) of the cristae in WT (left) and *ppargc1a*$^{sa13186/sa13186}$ mutant (right) zebrafish. Scale bar, 10 μm.
(E) Dorsal view of 3 dpf WT sibling (top) and *ppargc1a*$^{sa13186/sa13186}$ mutant (bottom) approximately 24 h after being injected with 40 kDa dextran-FITC to assay for pronephric function. White arrowheads indicate PCT fluorescence in WT. White box highlights the approximate area of the PCT with no fluorescence. Scale bar, 90 μm.
(F) Three days post-fertilization WT sibling (top) and *ppargc1a*$^{sa13186/sa13186}$ mutant (bottom) stained via WISH for *slc20a1a* to mark PCT. Scale bar, 90 μm.
(G) Fifty-five hours post-fertilization WT and *ppargc1a* MO injected zebrafish stained via WISH for the heart marker *myl7*. Penetrance graph of atypical heart looping occurring in WT and *ppargc1a* morphants. Chi-square analysis indicates significance. n = 128 (WT), n = 103 (MO), $p < 0.001$. Scale bar, 90 μm.
(H) Whole-mount immunofluorescence of the Kupffer's vesicle (KV) at the 10 ss stained for acetylated α-tubulin (cilia, green), anti-PKC (membrane boundary, red). Scale bar, 8 μm.
(I) Cilia length in micrometers of KV cilia.
(J) The number of cilia present in the KV.
(K) Twenty-four hours post-fertilization WT zebrafish stained via WISH to illustrate *ppargc1a* mRNA expression. Box is of approximate area of inset showing Ppargc1a (red) expression and the cilia marker acetylated α-tubulin (green). Scale bars, 65 μm for the whole embryo and 10 μm for the inset.
Data are represented as mean ± SD; **$p < 0.01$ and ***$p < 0.001$ (t test).

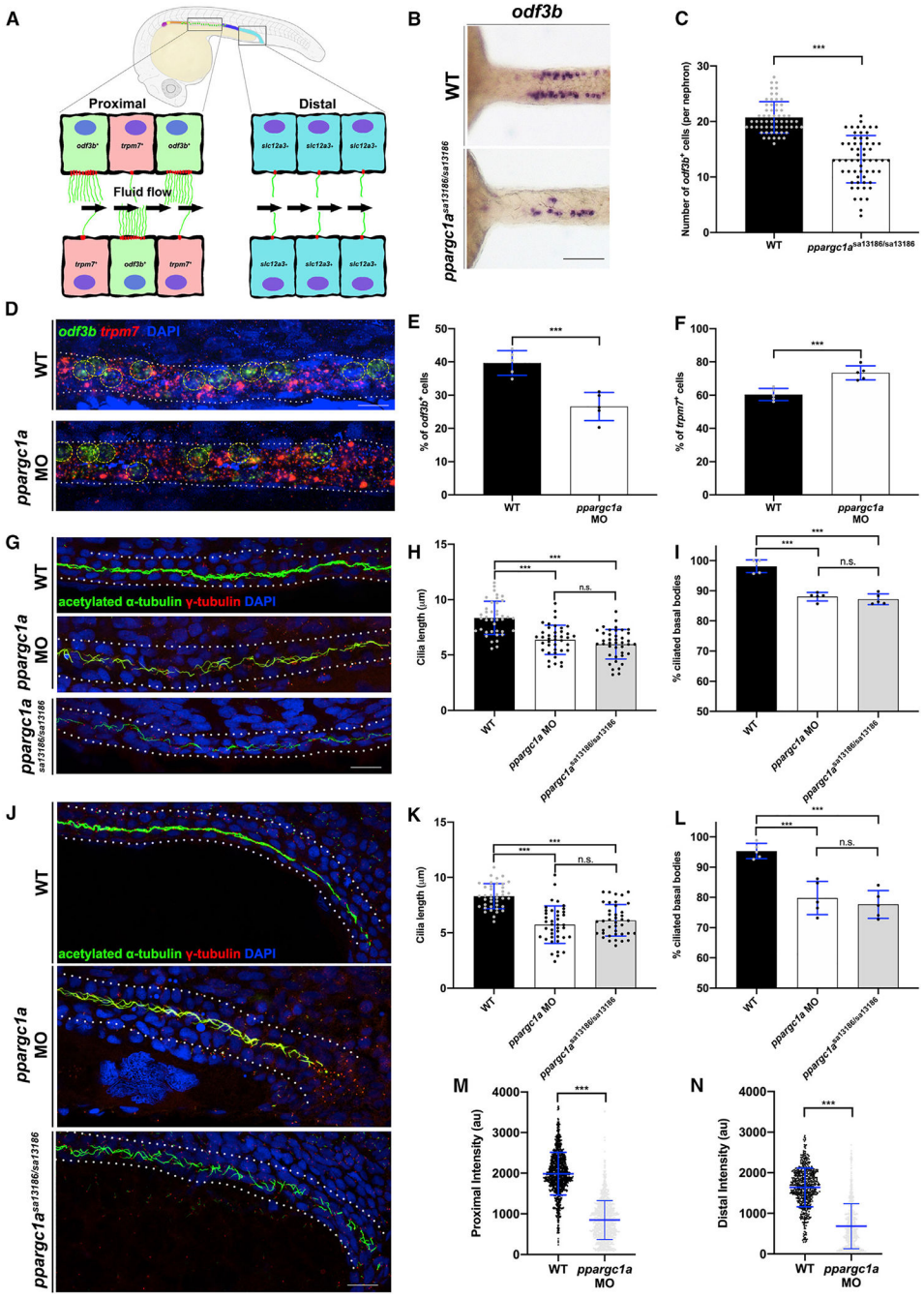

Figure 2. Loss of *ppargc1a* Results in Ciliogenesis Defects

(A) Schematic indicating location of MCCs in the proximal portion and monociliated cells in the distal portion of the zebrafish pronephros at 24 hpf.

(B) WT (top) and *ppargc1a*$^{sa13186/sa13186}$ mutant (bottom) zebrafish at 24 hpf stained via WISH for *odf3b* to mark MCCs. Scale bar, 90 μm.

(C) Graph representing the number of MCCs present in WT and *ppargc1a*^{sa13186}/sa13186 zebrafish at 24 hpf.

(D) Fluorescent *in situ* hybridization for MCC marker (*odf3b*, green) and transporter cell marker (*trpm7*, red) in WT and *ppargc1a* morphant zebrafish at 24 hpf. Scale bar, 10 μm.
(E and F) Graphs representing the percentage of *odf3b*$^{+}$ (E) or *trpm7*$^{+}$ (F) cells in WT (black) and *ppargc1a* morphants (white) pronephros between somites 9 and 11.
(G) Twenty-eight hours post-fertilization WT (top), *ppargc1a* MO-injected (middle), and *ppargc1a*$^{sa13186/sa13186}$ (bottom) zebrafish stained via whole-mount immunofluorescence for acetylated α-tubulin (cilia, green), γ-tubulin (basal bodies, red), and DAPI in the proximal pronephros. Scale bar, 10 μm.
(H) Cilia length in micrometers for the proximal pronephros.
(I) Graph of the percentage of ciliated basal bodies/total basal bodies per 100 μm in the proximal pronephros.
(J) Twenty-eight hours post-fertilization WT (top) and *ppargc1a* MO-injected (middle) and *ppargc1a*$^{sa13186/sa13186}$ (bottom) zebrafish stained via whole-mount immunofluorescence for acetylated α-tubulin (cilia, green), γ-tubulin (basal bodies, red), and DAPI in the distal pronephros. Scale bar, 10 μm.
(K) Cilia length in micrometers for the distal (right) pronephros.
(L) Graph of the percentage of ciliated basal bodies/total basal bodies per 100 μm in the distal pronephros.
(M and N) Fluorescent intensity plots of WT (black) and *ppargc1a* MO-injected (red) zebrafish in proximal (M) and distal (N) pronephros.
Data are represented as mean ± SD. *$p < 0.05$, **$p < 0.01$, and ***$p < 0.001$ (one-way ANOVA or t test).

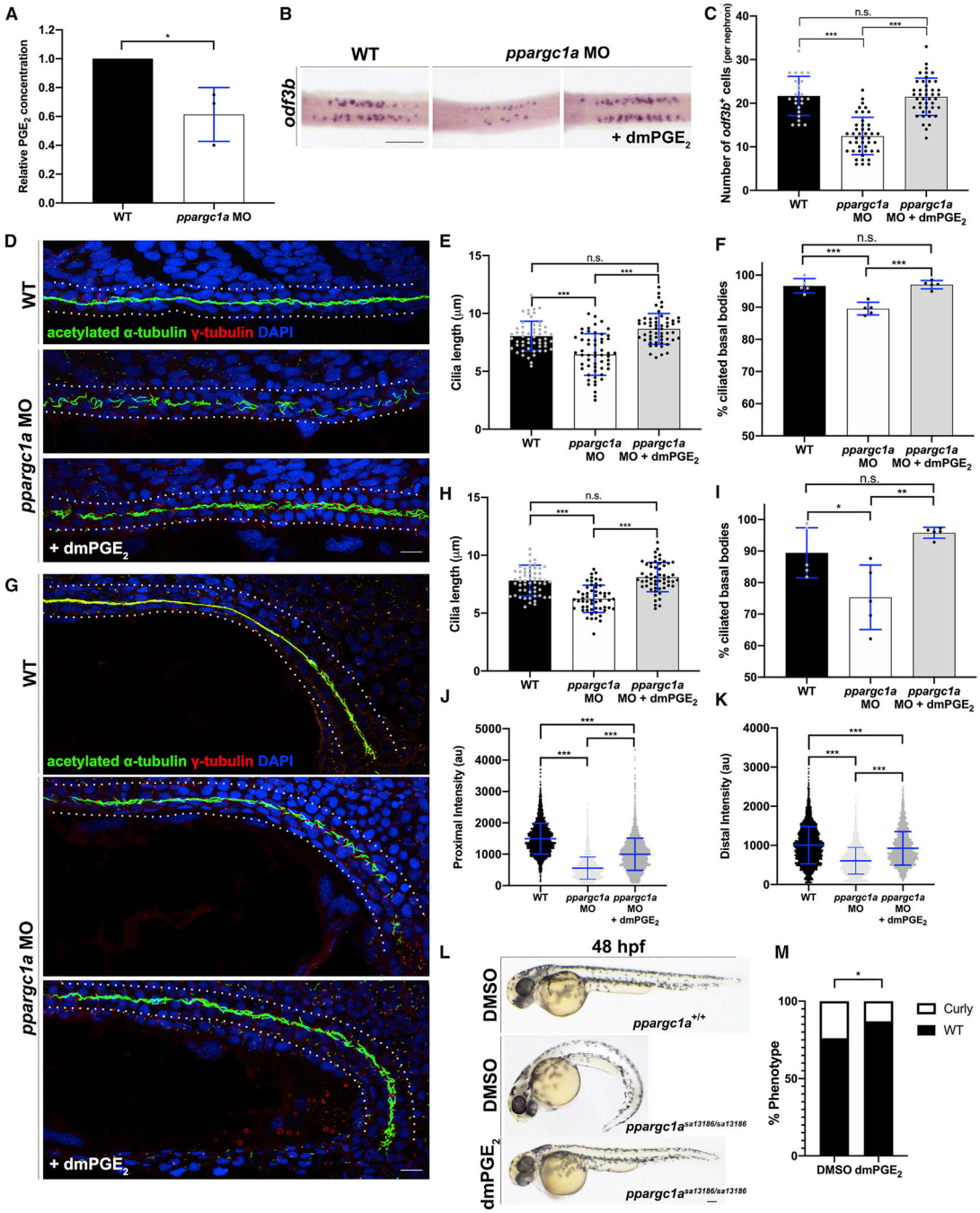

Figure 3. *ppargc1a* Loss of Function Phenotypes Can Be Rescued by Supplementing with PGE_2

(A) Relative concentration of PGE_2 in WT and *ppargc1a* morphants.

(B) MCCs stained via WISH for *odf3b* at 24 hpf in WT (left), *ppargc1a* MO (middle), and *ppargc1a* morphants treated with $dmPGE_2$ (right). Scale bar, 90 μm.

(C) Graph depicting the number of MCCs present in WT, *ppargc1a* MO, and *ppargc1a* MO treated with $dmPGE_2$.

(D) Twenty-eight hours post-fertilization WT (top), *ppargc1a* MO-injected (middle), and *ppargc1a* MO-injected + $dmPGE_2$ (bottom) zebrafish stained via whole-mount

immunofluorescence for acetylated α-tubulin (cilia, green), γ-tubulin (basal bodies, red), and DAPI in the proximal pronephros. Scale bar, 10 μm.

(E) Cilia length in micrometers for the proximal pronephros of WT, *ppargc1a* morphants, and *ppargc1a* morphants treated with $dmPGE_2$.

(F) Graph of the percentage of ciliated basal bodies/total basal bodies per 100 μm in the proximal pronephros.

(G) Twenty-eight hours post-fertilization WT (top), *ppargc1a* MO-injected (middle), and *ppargc1a* MO-injected + $dmPGE_2$ (bottom) zebrafish stained via whole-mount immunofluorescence for acetylated α-tubulin (cilia, green), γ-tubulin (basal bodies, red), and DAPI in the distal pronephros. Scale bar, 10 μm.

(H) Cilia length in micrometers for the distal pronephros of WT, *ppargc1a* morphants, and *ppargc1a* morphants treated with $dmPGE_2$.

(I) Graph of the percentage of ciliated basal bodies/total basal bodies per 100 μm in the distal pronephros.

(J and K) Scatterplots illustrating the difference in fluorescent intensity signals of WT, *ppargc1a* MO, and *ppargc1a* MO + $dmPGE_2$ in proximal (J) and distal (K) cilia.

(L) Representative images of $ppargc1a^{+/sa13186}$ in crosses shown at 48 hpf WT zebrafish treated with DMSO (top), curly $ppargc1a^{sa13186/sa13186}$ treated with DMSO (middle), and a WT-appearing, genotype-confirmed $ppargc1a^{sa13186/sa13186}$ rescued with $dmPGE_2$ (bottom). Scale bar, 90 μm.

(M) The percentage of zebrafish with WT (black) or curly (white) phenotypes at 48 hpf after treatment with DMSO or $dmPGE_2$. Chi-square test indicates significance.

Data are represented as mean ± SD. *$p < 0.05$, **$p < 0.01$, and ***$p < 0.001$ (one-way ANOVA or t test); n.s., not significant.

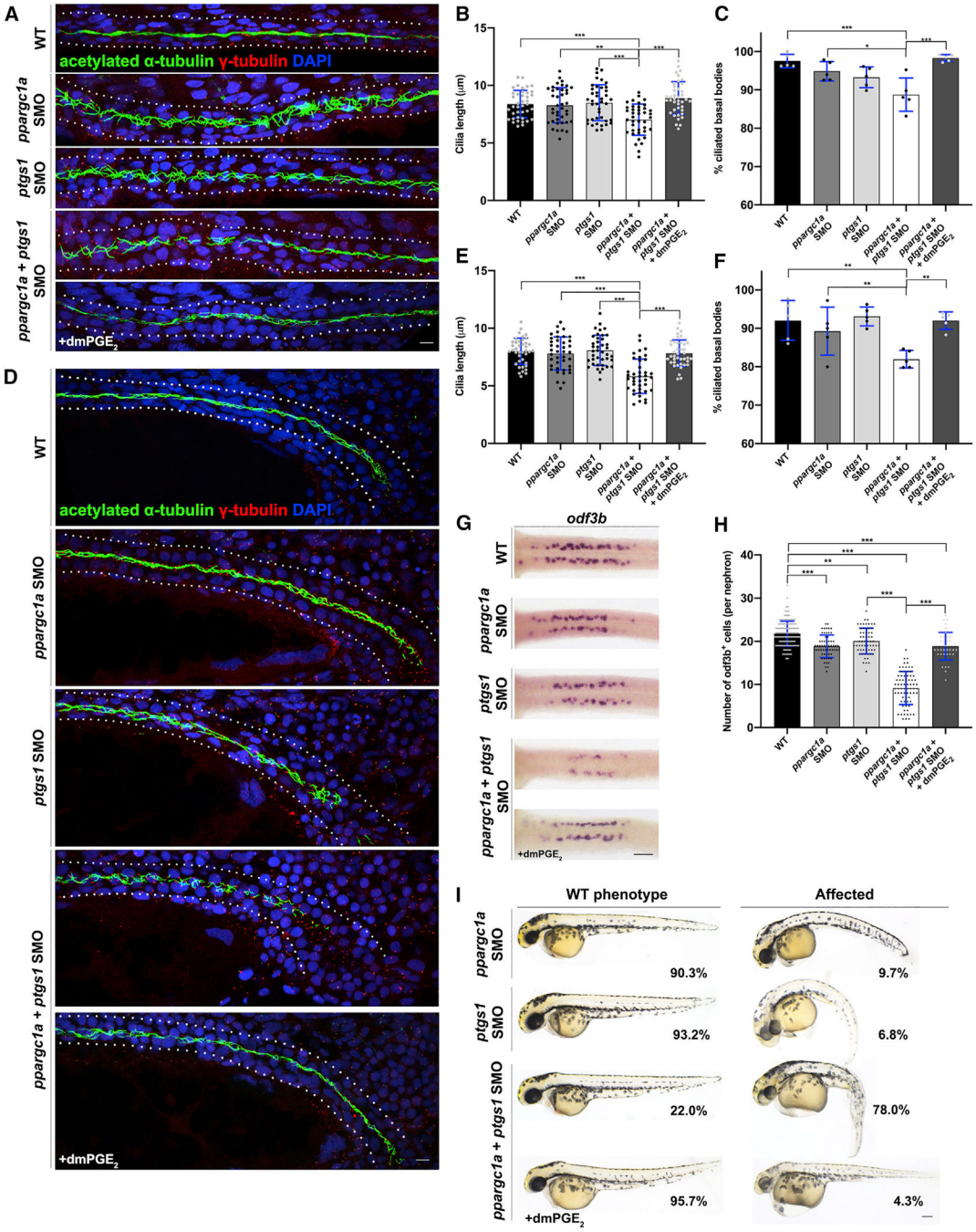

Figure 4. *ppargc1a* and Prostaglandin Pathway Component *ptgs1* Act Together to Properly Form Ciliated Cells

(A) Twenty-eight hours post-fertilization WT (top), *ppargc1a* suboptimal dose MO (SMO), *ptgs1* SMO, *ppargc1a* + *ptgs1* SMO, and *ppargc1a* + *ptgs1* SMO + $dmPGE_2$-treated zebrafish stained via whole-mount immunofluorescence for acetylated α-tubulin (cilia, green), γ-tubulin (basal bodies, red), and DAPI in the proximal pronephros. Scale bar, 7 μm.

(B) Cilia length in micrometers for the proximal pronephros.

(C) Graph of the percentage of ciliated basal bodies/total basal bodies per 100 μm in the proximal pronephros.

(D) Twenty-eight hours post-fertilization WT (top), *ppargc1a* SMO, *ptgs1* SMO, *ppargc1a* + *ptgs1* SMO, and *ppargc1a* + *ptgs1* SMO + $dmPGE_2$-treated zebrafish stained via whole-mount immunofluorescence for acetylated α-tubulin (cilia, green), γ-tubulin (basal bodies, red), and DAPI in the distal pronephros. Scale bar, 7 μm.
(E) Cilia length in micrometers for the distal pronephros.
(F) Graph of the percentage of ciliated basal bodies/total basal bodies per 100 μm in the distal pronephros.
(G) MCCs stained via WISH for *odf3b* at 24 hpf in WT, *ppargc1a* SMO, *ptgs1* SMO, *ppargc1a* + *ptgs1* SMO, and *ppargc1a* + *ptgs1* SMO + $dmPGE_2$-treated zebrafish. Scale bar, 50 μm.
(H) Graph depicting the number of MCCs present.
(I) Forty-eight hours post-fertilization zebrafish injected with *ppargc1a* SMO, *ptgs1* SMO, *ppargc1a* + *ptgs1* SMO, and *ppargc1a* + *ptgs1* SMO + $dmPGE_2$-treated displaying either a WT phenotype (left) or an affected phenotype (right). The respective penetrance is listed within each image area. Scale bar, 100 μm.
Data are represented as mean ± SD. *$p < 0.05$, **$p < 0.01$, and ***$p < 0.001$ (one-way ANOVA); n.s., not significant.

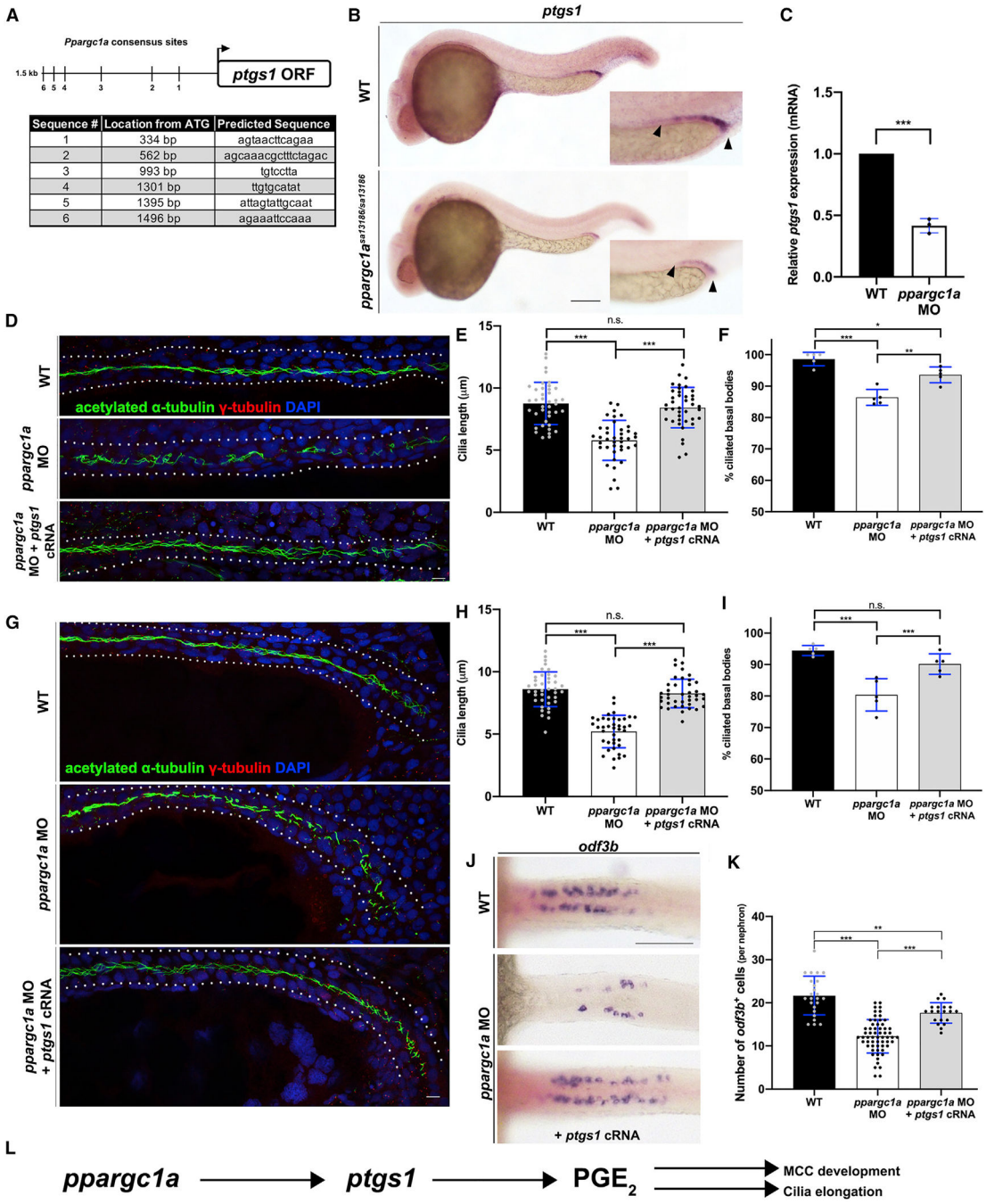

Figure 5. *ptgs1* Functions Downstream of *ppargc1a* during Ciliogenesis

(A) Schematic depicting several *Ppargc1a* consensus sites located within 1.5 kb of the *ptgs1* open reading frame (ORF).

(B) Twenty-four hours post-fertilization WT (top) and *ppargc1a*^{sa13186}/sa13186 (bottom) zebrafish stained via WISH for *ptgs1* (n > 60). Scale bar, 100 μm.

(C) Relative *ptgs1* mRNA expression in WT and *ppargc1a* morphants.

(D) Whole-mount immunofluorescence for acetylated α-tubulin (cilia, green), γ-tubulin (basal bodies, red), and DAPI in the proximal pronephros of WT (top), *ppargc1a* morphants (middle), and *ppargc1a* morphants injected with *ptgs1* cRNA (bottom). Scale bar, 7 μm.
(E) Cilia length for the proximal pronephros treatment groups shown in (D).
(F) Graph of the percentage of ciliated basal bodies/total basal bodies per 100 μm in the proximal pronephros.
(G) Whole-mount immunofluorescence for acetylated α-tubulin (cilia, green), γ-tubulin (basal bodies, red), and DAPI in the distal pronephros of WT (top), *ppargc1a* morphants (middle), and *ppargc1a* morphants injected with *ptgs1* cRNA (bottom). Scale bar, 7 μm.
(H) Cilia length for distal pronephros treatment groups shown in (G).
(I) Graph of the percentage of ciliated basal bodies/total basal bodies per 100 μm in the distal pronephros.
(J) WISH for the MCC marker *odf3b* in WT (top), *ppargc1a* morphants, and *ppargc1a* morphants injected with *ptgs1* cRNA (bottom). Scale bar, 90 μm.
(K) Number of MCCs per nephron.
(L) Proposed mechanism by which *ppargc1a* regulates MCC development and ciliogenesis via PGE_2 levels by controlling *ptgs1* expression.
Data are represented as mean ± SD. *$p < 0.05$, **$p < 0.01$, and ***$p < 0.001$ (one-way ANOVA or t test); n.s., not significant.

KEY RESOURCES TABLE

REAGENT or RESOURCE	SOURCE	IDENTIFIER
Antibodies		
Anti-tubulin acetylated	Sigma	T6793; RRID:AB_477585
Anti-γ-tubulin	Sigma	T5192; RRID:AB_261690
Anti-Ppargc1a	Abcam	AB54481; RRID:AB_881987
Anti-PKC	Santa Cruz	SC216; RRID:AB_2300359
Goat anti-Mouse IgG (H+L) Highly Cross-Adsorbed Secondary Antibody, Alexa Fluor 647	Invitrogen	A21236; RRID:AB_2535805
Goat anti-Rabbit IgG (H+L) Highly Cross-Adsorbed Secondary Antibody, Alexa Fluor 647	Invitrogen	A21245; RRID:AB_141775
Goat anti-Mouse IgG (H+L) Highly Cross-Adsorbed Secondary Antibody, Alexa Fluor 568	Invitrogen	A11031; RRID:AB_144696
Goat anti-Rabbit IgG (H+L) Highly Cross-Adsorbed Secondary Antibody, Alexa Fluor 594	Invitrogen	A11037; RRID:AB_2534095
Goat anti-Mouse IgG (H+L) Highly Cross-Adsorbed Secondary Antibody, Alexa Fluor 488	Invitrogen	A11029; RRID:AB_138404
Goat anti-Rabbit IgG (H+L) Highly Cross-Adsorbed Secondary Antibody, Alexa Fluor 488	Invitrogen	A11034; RRID:AB_2576217
Chemicals, Peptides, and Recombinant Proteins		
16,16-Dimethyl-prostaglandin E2	Santa Cruz Biotechnology, Inc	sc-201240
40 kDa dextran-FITC	Invitrogen	D-1845
Critical Commercial Assays		
Prostaglandin E2 Express ELISA Kit	Cayman Chemical	500141
mMESSAGE mMACHINE SP6 Transcription kit	Ambion	AM1340
PerfeCTa SYBR Green SuperMix with ROX	Quantabio	VWR 101414-160
qScript cDNA SuperMix	Quantabio	VWR 101414-106
TSA Plus Fluorescein	Akoya Biosciences	NEL741001KT
TSA Plus Cyanine	Akoya Biosciences	NEL744001KT
Experimental Models: Organisms/Strains		
ppargc1a-sa13186	ZIRC	N/A
Oligonucleotides		
ppargc1a qRT-PCR forward AATGCCAGTGATCAGAGCTGTCCTT	This paper	N/A
ppargc1a qRT-PCR reverse GTTCTGTGCCTTGCCACCTGGGTAT	This paper	N/A
18S qRT-PCR forward TCGGCTACCACATCCAAGGAAGGCAGC	This paper	N/A
18S qRT-PCR reverse TTGCTGGAATTACCGCGGCTGCTGGCA	This paper	N/A
ptgs1 qRT-PCR forward CATGCACAGGTCAAAATGAGTT	This paper	N/A
ptgs1 qRT-PCR reverse TGTGAGGATCGATGTGTTGAAT	This paper	N/A
ppargc1a-sa13186 genotyping forward primer GGGCCGGCATGT GGAATGTAAAGACTTAAACATGCCAACCTCCACTACTACGACAT ATCGTTGTCTTCCACCCCCCCTTCGTCTTCCTCACTGGCCAGG	Chambers et al., 2018	N/A

REAGENT or RESOURCE	SOURCE	IDENTIFIER
ppargc1a-sa13186 genotyping reverse primer TCCCACTACCCCG CTATAGAAGGCTTGCTGAGGCTTTCCAAAGTGCTTGTTGAGCTC GTCCCGGATCTCCTGGTCCCTAAGAAGTTTCCTGCCACCAGAA	Chambers et al., 2018	N/A
ppargc1a morpholino CCTGATTACACCTGTCCCACGCCAT	Gene-Tools	ZFIN: MO1-ppargc1a
ptgs1 morpholino TCAGCAAAAAGTTACACTCTCTCAT	Gene-Tools	N/A
standard control morpholino. CCTCTTACCTCAGTTACAATTTATA	Gene-Tools	N/A
ift88 morpholino AGCAGATGCAAAATGACTCACTGGG	Gene-Tools	N/A
Software and Algorithms		
Prism v8	Graphpad	https://www.graphpad.com/scientific-software/prism/
ImageJ	Fiji	ImageJ (https://imagej.nih.gov/ij/)